Master of Science Thesis
VT2015

Developement of a portable β-spectrometer for in situ measurements of Sr-90 and Y-90 using a plastic scintillator and a silicon photomultipler (SiPM).

Daniel Krona

Supervision

Lars Herrnsdorf and Sören Mattsson, Malmö

This work has been conducted at
Medical Radiation Physics, Skåne University Hospital, Malmö

Department of Medical Radiation Physics,
Clinical Sciences, Lund
Lund University
www.msf.lu.se

Abstract

In the event of a nuclear weapon detonation or a power plant accident radionuclides will deposit on the ground. It is then important to identify and quantify the radionuclides to obtain information necessary for radiation protection efforts like relocation and decontamination. Radiation protection instruments with beta probes can be used as search instruments but the small surface of the probe and the lack of separation of beta energy are limitations concerning identification and quantification of the important radionuclide Sr-90. The present alternative for Sr-90 analysis is to collect grass and soil samples and perform time consuming radiochemistry and measurements.

Using a plastic scintillation detector, Sr-90 and the daughter radionuclide yttrium-90 can be identified and quantified. Sr-90 is of special interest due to its uptake and accumulation in the human skeleton. The high beta energy from Y-90 can be utilised to discriminate this radionuclide from other pure beta emitting radionuclides with lower beta energies.

Photomultiplier tubes (PMT) have been the common choice for light collection from scintillating materials for a long period of time. The development of alternatives has been successful the last years in form of silicon photomultipliers (SiPM). Silicon photomultiplier is a photodiode consisting of multiple cells operating in Geiger mode.

The setup consisted of a 15 mm thick plastic scintillator disc where a 1.5 meter long wavelength shifting fibre was wired around the edge surfaces and coupled to a SiPM mounted in a power supply and amplification unit. The signal was processed by a digitizer and the data was analysed using a laptop PC.

The measurements were performed with a Sr-90/Y-90 source, a Cs-137 source and a Co-60 source. Uniformity, protection from ambient light, temperature dependence was investigated. The SiPM sensitivity to beta particles was tested by exposing the SiPM to Sr-90/Y-90 without a detector. The evaluation of the CAEN SP5600 kit was done by using the mini spectrometer and the three detectors for collection of spectra from Sr-90/Y-90 and Cs-137.

The setup was not totally light tight, but the ambient light wouldn't disturb the measurements of radionuclides. The setup was uniform regarding collection of beta particles from a Sr-90/Y-90 source, but the SiPM could yield a signal if it was hit by beta particles directly. The detection limit is currently relatively high, but there is a potential for considerable improvements.

Regarding the evaluation of the CAEN SP5600 kit, the associated mini spectrometer containing a 3 x 3 mm^2 SiPM and three different types of detectors were used. This resulted in low detection limits and easy identification and quantification of Sr-90/Y-90. The conclusion is that it is possible to measure Sr-90/Y-90 using a plastic scintillator and a SiPM under laboratory conditions.

Populärvetenskaplig sammanfattning

Om ett kärnvapen detoneras i atmosfären eller en allvarlig kärnkräftsolycka, likt Tjernobyl, inträffar kommer radioaktivt nedfall att ske. Nedfallet innehåller radioaktiva ämnen som kommer att spridas ut över ett stort område med vind eller nederbörd. Vid denna situation är det viktigt att kunna identifiera vilka radioaktiva ämnen som finns på marken samt vilken radioaktivitet dessa har för att kunna avgöra vilka åtgärder som behövs sättas in för att minimera stråldosen till människan och omgivningen. Speciellt viktig att identifiera och kvantifiera är betastrålaren strontium-90 eftersom denna radionuklid inte ger något utslag vid de mätningar som normalt görs efter ett nedfall. Strontium-90 tas även upp i skelettet och ger därmed en hög stråldos till benmärgen som är extra strålkänslig.

De nuvarande strålningsdetektorerna som används för att spåra betastrålare har en liten yta och kan inte separera de olika radioaktiva ämnena. Genom att utnyttja att strontium-90 sönderfaller till yttrium-90 kan man detektera yttrium-90 som har mycket hög partikelenergi och då få information om strontium-90. En strålningsdetektoruppställning som skulle kunna användas består av en plastscintillator, en optisk fiber och en ljusdetektor. När partiklar från radioaktiva ämnen träffar plastscintillator interagerar partiklarna med materialet och scintillationsljus sänds ut. Detta ljus samlas upp av en optisk fiber och leder det till ljusdetektorn som konverterar ljuset till en signal som en dator kan hantera där då resultatet ses.

För att testa om detektoruppställningen fungerar bra har det gjorts mätningar på de vanligaste och mest relevanta radioaktiva ämnena. Det har också testats om detektorn är lika känslig över hela ingångsytan för partiklarna och om mätningarna störs av omgivande ljus. Angående ljusdetektorn har det testats om den är beroende av temperatur samt om partiklar som träffar ljusdetektorn direkt kan påverka mätningarna.

Resultatet av examensarbetet visar att det är möjligt att detektera strontium-90 och yttrium-90 även om dessa omges av andra radioaktiva ämnen. Detektorn är lika känslig över hela ingångsytan och är inte helt ljustät, men det omgivande ljuset stör inte mätningar avsevärt. Ljusdetektorn var temperaturberoende och därför är det att föredra att vänta tills temperaturen i elektroniken har stabiliserats. Partiklar som träffar ljusdetektorn direkt kan komma att störa mätningarna. En uppställning med en längre optisk fiber där plastscintillator och ljusdetektor mer separerade hade kunnat minska denna effekt.

Acknowledgements

Through the donation of the CAEN equipment by Maria and Lars Herrnsdorf to Medical Radiation Physics in Malmö my work was made possible. I hope this donation will encourage future research and education involving SiPM.

I wish to express my sincere thanks to my supervisors Lars Herrnsdorf and Sören Mattsson for the continuous encouragement and support.

I am grateful to Karl Östlund for sharing expertise and valuable guidance concerning detectors and fibres.

I´d like to thank Stefan Isaksson at Gammadata, Uppsala, for providing the WLS-fibre and sharing expertise regarding light reflection and light protection of the scintillation detector.

I´d like to thank Mikael Andersson at Micropol, Åled, for great discussions and input about the use of optical fibres and also the good work of applying the optical fibre connectors to the WLS-fibre.

I also like to thank Jonas Nilsson and Jonas Jarneborn for sharing office space and good input and discussions regarding the progress of this work.

Finally I´d like to direct thanks to Marcus Persson for discussing upcoming problems and new ideas.

Contents

1. Introduction

1.1 Background

In the event of a major nuclear power plant accident, radionuclides will deposit on the ground. It is then important to identify and quantify the radionuclides to obtain information necessary for radiation protection efforts and decontamination. Using field-gamma spectrometry gamma emitting radionuclides can be detected and quantified. For pure beta emitters, the situation is more difficult.

Radiation protection instruments with beta probes can be used as search instruments for beta contamination *in situ* but the small surface of the probe, the lack of separation of beta energy and sensitivity for gamma radiation are limitations concerning identification and quantification. The present alternative for strontium-90 analysis is to collect grass and soil samples and perform radiochemical analysis. This is time consuming, order of several days, which is not acceptable in a situation when fast results are necessary [1].

With a plastic scintillator detector, Sr-90 and the daughter nuclide yttrium-90 can be identified and quantified [2]. Among the pure beta emitters Sr-90 is of special interest due to its uptake and accumulation in the human body. To detect beta particles from Sr-90 and Y-90 a detector that can handle high dose rates is required. The high beta energy from Y-90 can be utilised to discriminate this radionuclide from other pure beta emitting radionuclides with lower beta energies. Plastic scintillators with fast readout and electronics are an option and could be suitable to use in this situation [3].

Photomultiplier tubes (PMT) have been the common choice for light collection from scintillating materials for a long period of time. The advantages are linear charge amplification and the disadvantages are its bulky size and sensitivity to shocks, vibrations and magnetic fields [4].

The development of alternatives for the PMT has been successful the last years in form of silicon photomultipliers (SiPM). Silicon photomultiplier is a photodiode consisting of multiple cells operating in Geiger mode. The performance have been improved a lot during the last few years but it still has disadvantages including high dark count rate, demands cooling to remain stable and has a small surface area [4].

1.2 Aim

The purpose was to investigate the possibility to assemble a portable beta spectrometer with the capacity to measure Sr-90 and Y-90 *in situ* using a plastic scintillator and a SiPM. Light protection, detection limits, detection uniformity and disturbances from other radionuclides present in the fallout should be investigated under laboratory conditions. An evaluation of the CAEN SP5600 kit should also be performed regarding the property of processing the signal received from a SiPM.

2. Background

2.1 Fallout

Historically radioactive fallout has occurred after nuclear weapons tests and nuclear power plant failures. The testing of nuclear weapons in the atmosphere was especially intense during 1957-58 and 1961-62 [5]. The most severe nuclear power plant accidents that lead to fallout are Chernobyl in 1986, Fukushima Daiichi in 2011, Kyshtym (Mayak, Russia) in 1957 and Windscale (Great Britain) in 1957 [5].

The largest sources of artificial radioactivity from a nuclear accident are nuclear fission of heavy nuclei like U-235 and Pu-239. These nuclides undergo fission with thermal neutrons and fast neutrons in a nuclear reactor. The most probable process with thermal neutrons in nuclear fission is the creation of two fragments of different size, due to that the maximum fission yield occurs at mass number 95 and 138 for U-235 [5].

Nuclear weapons are often detonated underground and only a small fraction is spread to the atmosphere. In case of an atmospheric explosion all of the radioactive products are released in the atmosphere. The detonation produces several radioactive nuclides where fission products, residuals of the fissile material and also other nuclides created by activation of the components of the device, as well as in the ground and air, are released. After a 1 kT nuclear explosion approximately 10 TBq Sr-90, 10 TBq Cs-137 and 1 GBq Cs-134 are released [6].

From a power plant accident or a detonation of a nuclear weapon in the atmosphere radionuclides will spread with the air and deposit on the ground through dry deposition or rain. The most common and important nuclides from a radiation protection perspective are Cs-137, Cs-134, I-131 and Sr-90 [5].

Due to their chemical properties the radionuclides incorporates quickly in the environment. The long physical half-life of Sr-90 and Cs-137 is leading to that these nuclides will be present in the environment for a long time. Humans are affected by the radionuclides through external irradiation and through food and drinks where the intake leads to accumulation in the body. I-131 reaches the human body by intake of fresh milk and leafy vegetables and is accumulated in the thyroid. Cs-134 and Cs-137 are chemically similar to potassium and are accumulated in muscle tissue and soft tissue. Sr-90 is from a radiological perspective important due to the similarities to calcium and is accumulated in the skeleton where the effective half-life is long [5].

2.2 Strontium-90

The radioactive isotope Sr-90 has a physical half-life of 28.79 years and decays to Y-90 and emits a beta particle with maximum energy of 546 keV. The daughter Y-90 has a half-life of 64.0 hours and decays to the stable Zr-90 and emits a beta particle with maximum energy of 2.28 MeV [7].

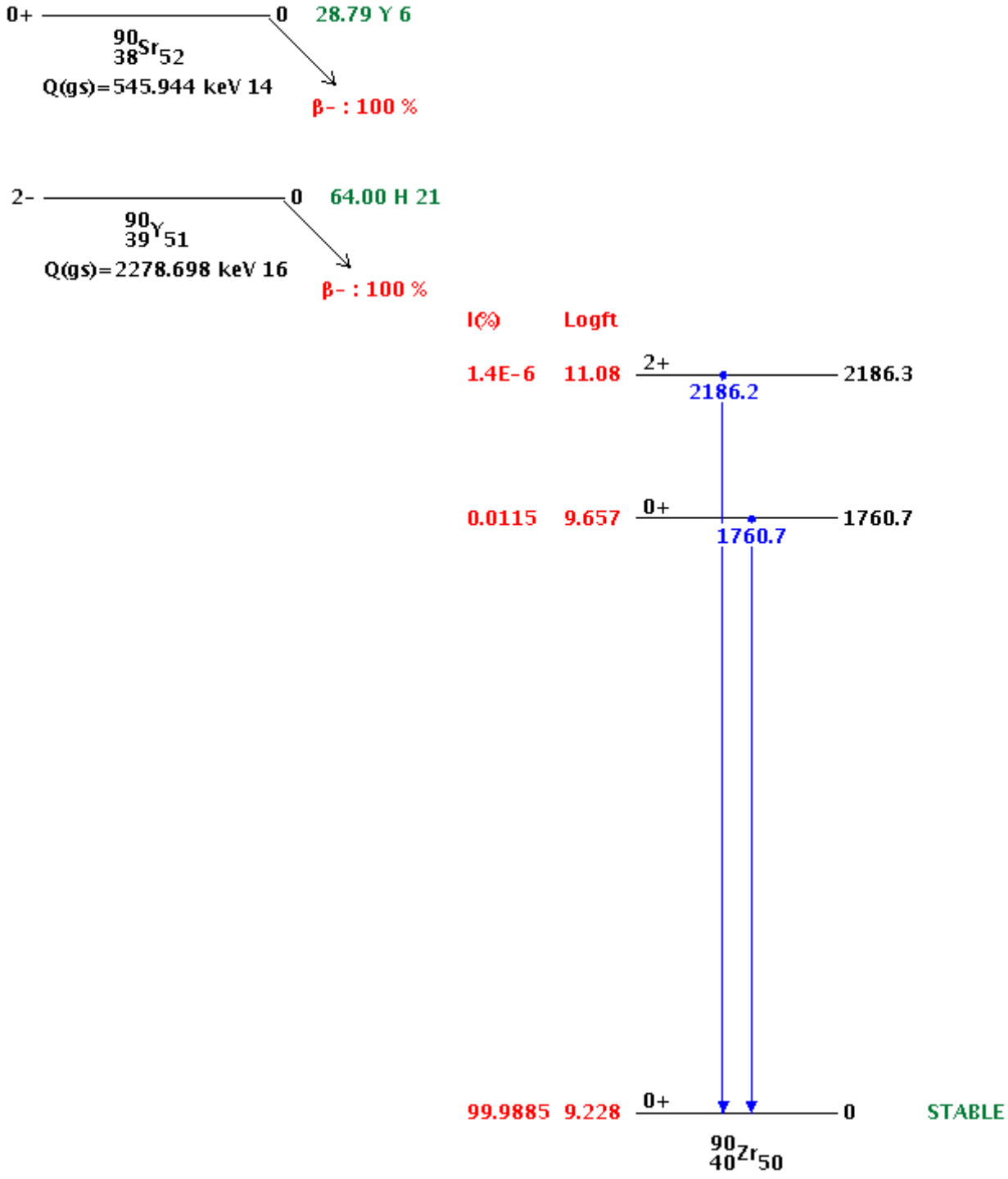

Figure 1. Decay scheme of Sr-90 and Y-90 [7].

The quantities of Sr-90 released during various accidents are identified in Table 1.

Table 1.Quantities of Sr-90 released from accidents.

Location and year	Chernobyl, 1986	Windscale, 1957	Kyshtym, 1957	Lake Karachay, 1951-1978	Soviet Satellite, 1978	Fukushima Daiichi, 2011 (over sea)
Activity released [Bq]	Ca. $10 \cdot 10^{15}$ [5]	$220 \cdot 10^{9}$ [5]	$2 \cdot 10^{15}$ [5]	$4 \cdot 10^{18}$ [5]	$3 \cdot 10^{12}$ [5]	$90\text{-}900 \cdot 10^{12}$ [8]

Sr-90 is causing direct contamination of vegetables, crops, grass and surface water. Sr-90 is mobile in the ground where it migrates vertically with time and is absorbed by the plant's roots and is then spread to man directly or indirectly through animals [5]. When accumulation of Sr-90 in the skeleton occurs, the high energy of the beta particles from Y-90 contribute to a high absorbed dose to bone, bone marrow and surrounding tissue.

2.2.1 Beta particle interaction and range

The beta particles emitted by a radionuclide have a continuous energy distribution. Interacting with a material the low-energy beta particles are rapidly absorbed. The shape of the attenuation curve is near-exponential but the description of the behaviour is only an empirical approximation [4].

CSDA range, R_{CSDA}, is the continuous slowing down approximation and is defined as

$$R_{CSDA} = \int_0^{T_0} \left(\frac{dT}{\rho dx}\right)^{-1} dT \quad (1)$$

where T_0 is the starting energy of the particle. If $dT/\rho dx$ is in MeV cm^2/g and dT in MeV then R_{CSDA} is given in g/cm^2 [9]. Multiplying the R_{CSDA} with the density of the material the particle is entering, the range in cm is given.

2.3 Scintillating material

When gamma photons, beta particles and neutrons interact with a scintillating material scintillation light is emitted isotropically from the particle track. The scintillation process consists of two processes, fluorescence and phosphorescence. Fluorescence is the process where an incoming photon excites an atom by absorption and the atom is emitting light when the atom is deexciting. Phosphorescence is the process where the light doesn't emit promptly after excitation and emits light with longer wavelength than the fluorescence. A competing process is the delayed fluorescence that emits the same spectrum as prompt fluorescence, but characterizes of a longer emission time after excitation [4].

A good scintillating material should have a large conversion efficiency of incoming energy from radiation to prompt fluorescence with as little contribution from phosphorescence and delayed fluorescence as possible. The light that is contributing to an electronic pulse is

generally limited to prompt fluorescence due to the shorter shaping time compared to phosphorescence and delayed fluorescence. The long-lived light is spreading randomly in time between signal pulses and arrives to the photomultiplier as individual photons and can often not be separated from noise [4].

The effectivity is important and the scintillator efficiency is defined as the ratio between the sum of the energy of visible light and the sum of the incoming particle energies.

$$Scintillator\ effeciency = \frac{\sum visible\ light}{\sum Particle\ energy} \quad (2)$$

This should be as large as possible but all deexcitations don't emit light and instead leads to energy in form of heat [4].

The response of the scintillator from beta particles depends on the scintillation material, the physical thickness and the angle of incidence of the particles. The beta particles must pass a protective cover, often including reflective material and light protective material, before entering the scintillator surface. The low energy beta particles will then be attenuated and doesn't reach the scintillator. To maximize the scintillator efficiency the physical thickness must be larger than the range of the beta particles of interest. A thicker scintillator is also leading to more detected bremsstrahlung photons generated from the path of the electron and other gamma rays from the surroundings. The expected spectrum from a beta source is a typical beta spectrum with addition of bremsstrahlung [4].

Many different types of material have the ability to emit scintillation light when exposed to radiation. The scintillating material is divided in two categories, organic and inorganic scintillators, where the difference is the crystal structure. The organic scintillation material, where plastic is included, has a faster decay of the scintillation light but have lower light yield compared to inorganic material. The content of hydrogen and low sensitivity for gamma photons of organic scintillating material makes it suitable for beta spectroscopy and fast detection of neutrons [4].

Independent of category, the ideal scintillation material should convert kinetic energy of charged particles to detectable light with high efficiency and possess a light yield that is proportional to deposited energy over as wide range as possible. The material should also be transparent to the wavelength of its own emission for good light collection, have a short decay time of the induced luminescence so that fast signal pulses can be generated, a good optical quality and be suitable to manufacture in sizes large enough to be of interest as a practical detector. For efficient optical coupling of the scintillation light to a photomultiplier tube or other light sensor the index of refraction of the materials should be near glass (~1.5). Another preferable property of a scintillating material is that the light should easily be converted to an electric pulse [4].

No scintillating material has all these properties and the choice of material is always a compromise. The low atomic number of the organic scintillating material makes it not suitable for gamma spectrometry but more suitable for neutron and beta detection [4]. One type of scintillating material is plastic and the advantage is that it can be shaped in many

different forms and it´s cheap to manufacture. It has also low atomic number and this makes it insensitive to photon radiation [4].

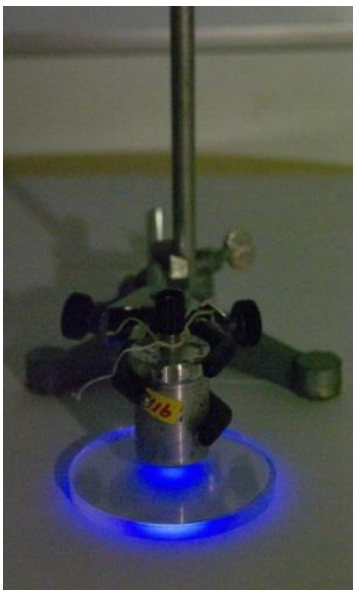

Figure 2. 69.1 MBq collimated Sr-90 source generating scintillation light in the plastic scintillator NE102A. The scintillator is polished at the top and bottom area and unpolished at the side area. The exposure time of the camera was set to 304 seconds.

2.4 Light guide

The optimal light guide collects all scintillation light created in the scintillating material and is guiding it to the light detector without losses. This is often difficult where there is a challenge to optically couple the surface of the scintillating material to a light detector. The shape of the scintillating material doesn't always fit the shape of the light detector and the difference in sizes is going to be a problem. A common solution is to use polymethyl methacrylate (PMMA) that is easy to shape and cheap. Other effects leading to lower light collection is optical self-absorption in the scintillating material and escaping light. [4].

To minimize the amount of light escaping from the scintillating material the surfaces of the detector that is not used for light collection are often treated with a reflective coating. This can be done with reflective paint or other materials with good reflective abilities. With this surface treatment the scintillation light hitting the scintillator surface will be reflected and be guided by the light guide to a greater extent.

2.4.1 WLS-fibre

Wavelength shifting fibres (WLS-fibres) are optical fibres doped with a wavelength shifter. As a wavelength shifter, fluorescent dye is used. The incoming light is absorbed by the fluorescent dye and the energy is then emitted as light with longer wavelength. This light, often green, is partially trapped within the fibre by total internal reflection [10]. The trapping efficiency is dependent on the type of fibre, but Saint-Gobain promises a minimum of 3.44 % [11]. The light is also attenuated in the fibre on its way to the ends of the fibre. A large fibre diameter will maximize the capture fraction, but is limiting the loop radius. This fibre can be used as a guide for scintillation light and is an efficient way to concentrate light into a small area like a photo detector [10].

2.5 Light collection

The aim is to collect as much of the emitted scintillation light as possible. The most common choice is photomultiplier tube that uses a photocathode material to eject electrons and multiply these until a measurable current is reached. Lately photodiodes have been improved to be used as collectors of scintillation light.

2.5.1 Photodiodes

A photodiode is a semiconductor device that converts light into current. A conventional photodiode works in the way that when a photon absorbed in the depletion layer between the p-layer and the n-layer an electron-hole pair is generated. The electron is affected by the electric field and is swept to the positive n-layer and the current is proportional to the light.

2.5.2 Avalanche diodes

Photodiodes using the avalanche process is called avalanche photodiodes (APD). The objective is to collect all charge carriers that are created by the incident radiation within the active volume and achieve charge multiplication. Gain is achieved within the semiconductor material, often silicon, by applying an electric field to a level high enough to enable the migrating electrons to create secondary ionization during the collection process. The avalanche detectors must allow the generation of high fields within the volume of the detector allowing the field at the surface to become so large as to create surface breakdown. Gains of up to several hundred in total collected charge are possible but there has been some difficulty in achieving uniform multiplication across the entire entrance window. The gain is also strongly dependent of applied voltage and temperature and stable operation requires attention to this. Charge carriers created within the high-field region will be multiplied by a variable gain depending on their position relative to the boundaries. The configuration often provides a normal drift region where the electric field is too low to create multiplication. Then a more uniform multiplication of the charge is expected [4].

Avalanche photodiodes are manufactured in different ways but a common choice is a configuration where the light enters a thin p+ layer and interacts in a thick active region π. This creates electron-hole pairs and electrons are drawn through drift portion and into the multiplying region where a high electric field exists. The electrons are drawn through the high field region and create more electron-hole pairs in the multiplication process. The electrons will continue in the same direction but the holes will go in the opposite direction. At sufficient high field values, the holes can multiply and the hole multiplication produces more free electrons and leads to a runaway. This occurs at the breakdown voltage and the applied voltage is often kept slightly below this level. In this region the overall gain will be an exponential function of applied voltage accounting for the extreme sensitivity to applied voltage. The gain factor is about a few hundred leading to increased measured signal. The enhancement of the signal is sufficient to allow much lower light level to be sensed or lower energies measured in use of scintillators [4].

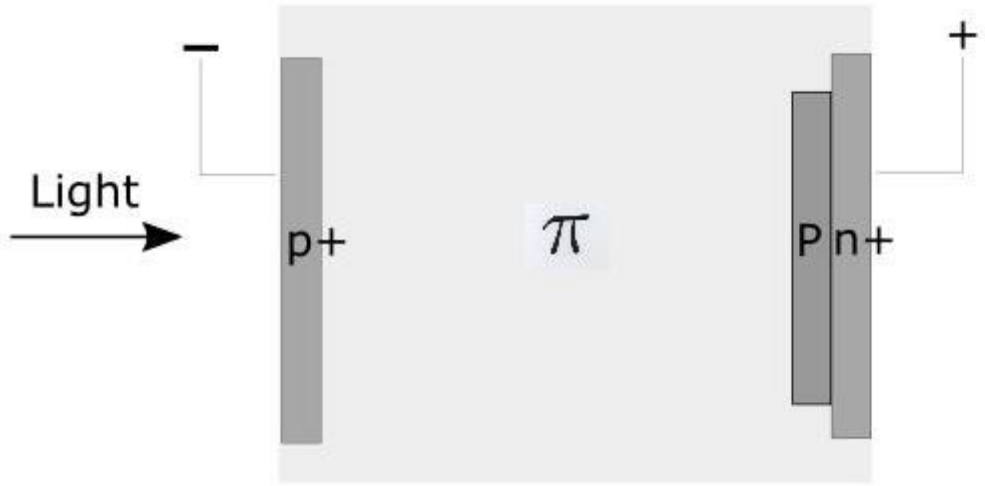

Figure 3. A common configuration of an avalanche photodiode.

The multiplication process in an avalanche diode involves electrons undergoing collisions at random positions throughout the avalanche. When an ionization collisions occurs one free electron is increased to two. Compared to a photo multiplier tube the peak to peak fluctuations in gain are significant. The fluctuations of the gain in a PM tube are becoming less significant with higher gain per dynode. Avalanche multiplication can be thought of as having a gain per dynode of 2, much lower compared to photomultiplier tube, and the fluctuations can be expected to be larger. When APD are used with scintillators the energy resolution can be affected negatively. The electronic noises are present and can also affect the overall energy resolution. These disadvantages can be helped by the superior quantum efficiency and has shown good energy resolution with small scintillators. Larger APD is not available so testing with these optically coupled directly to a larger crystal is not possible due to the poor light collection efficiency. The electronic noise is the superior problem so the resolution at low energies becomes inferior at a comparison. [4]

The statistics of the signal from an avalanche photodiode is very alike as for the proportional counter where pulse to pulse fluctuations arises from two independent statistical effects; variation of number of electron-hole pairs for fixed energy depositions in the scintillator and stochastic differences in the multiplication process. Lowest fluctuations are obtained with low applied voltage and gain values but at the expense of lower signal amplitude and signal-to-noise ratio. [4].

A quantum efficiency up to 80 % can be achieved using an antireflective coating on the external surface of the photodiode. The peak wavelength is often at 500-600 nm but newer generations have a peak wavelength of 400-500 nm due to the demand of sensitivity of blue light from scintillators. The sensitivity is important when using scintillators and this is maximized by applying this antireflective coating and minimizing the dead layer thickness of the surface [4].

Using fast scintillators, a timing resolution under a nanosecond can be obtained but is more often few nanoseconds or more. The gain providing higher signal, shorter shaping times can

be used with avalanche diodes and compared to conventional photodiodes higher count rates and better timing resolution can be achieved [4].

2.5.3 Silicon photomultipliers

Silicon photomultipliers (SiPM) have many names, multi pixel photon counter (MPPC) or solid state photomultiplier (SSPM) and consists of a matrix of many small avalanche diodes. Each small avalanche photodiode cell has dimensions of tens of microns produced using CMOS (complementary metal oxide semiconductor) processes on a silicon chip. It is wanted that the size of the cell is small so that not more than a single photon is incident on a cell simultaneously. The number of cells producing an avalanche is proportional to the number of incident scintillation photons. The number of cells must be a large multiple of the number of collected photons due to the amount of light photons produced by a scintillation detector. For this purpose, matrixes with 10^4 or more is not unusual. The cells are connected in parallel and produce an analogue pulse where the amplitude is proportional to the number of detected photons [4].

Silicon photomultipliers are very sensitive to single photoelectrons but is also responsive to conduction band electrons generated thermally in the silicon. This adds random noise to the scintillation signal. The dark pulse rate can be as large as 10^6 pulses per second per mm^2 and the cause is often hitting a single cell. Setting a discrimination level corresponding to the hitting of multiple cells, the dark count rate will be many times lower. This discrimination level should be suitable for scintillation light due to the large amount of light photons incident on the matrix at each pulse. Noise is also added by the contribution of thermal electrons which can be reduced by cooling [4].

The dark noise of the SiPM also includes afterpulsing and optical cross-talk. Afterpulsing occurs when impurities in the silicon lattice act as traps that deexcite with time. The electrons from the traps may cause following avalanches within the same cell and increase the number of avalanches per scintillation photon. Optical cross-talk occurs due to fluorescence initiated by avalanches where photons emitted from the cell trigger avalanches in adjacent cells. A larger fill factor gives higher probability to initiate following avalanches. A solution to this is the manufacturing of opaque trenches between the pixels. When a reflective wrapped scintillator is mated to the SiPM, avalanche photons may reflect inside the scintillator and overcome any inter-cell barrier. The statistics of the optical cross-talk noise will then also depend on the optical characteristics of the scintillator. The noise of the SiPM is an interplay of scintillation light, thermal electrons, afterpulsing and optical cross talk [4].

Among the operational properties the photon detection efficiency (PDE) of the SiPM are very important. It´s defined as the product of the geometric fill factor, the quantum efficiency and the avalanche initiation probability.

$$PDE = GFF \cdot QE \cdot AIP \tag{3}$$

The geometric fill factor is the ratio of the light sensitive area and the geometrical area. The quantum efficiency is defined as the probability of the creation of a photoelectron from a photon entering the device. It is dependent on the scintillation photon wavelength and related

to the optical absorption coefficient of the semiconductor substrate. The avalanche initiation probability is related to the extinction probability for branching processes. The probability of an avalanche forming a full discharge is higher when the electric field is increased by increasing the bias voltage [4].

Advantages of the silicon photomultipliers compared with the photomultiplier tubes are low operating voltage and the compact form. The challenges with the silicon photomultipliers are thermal noise and strong dependence of gain, noise and photon detection efficiency on temperature and voltage. To be able to make stable measurements a system must be used that measures or compensates for the fluctuations [4]. The small surface size available is also a disadvantage when a large scintillation crystal is used.

Visualize the scenario of a flash of light, with short time duration compared to the recovery time of a cell, uniformly illuminates the silicon photomultipliers surface. If the probability of hitting a specific cell is 10 % then it is a 1 % probability that two photons capable of triggering the cell will arrive within its resolving time. The size of the cell output is the same as for a single photon so some photons are lost by this random process and the silicon photomultipliers output pulse will fall short of the amplitude that will be produced if each photon had triggered an individual cell. The loss will increase with intensity of the light flash so a measurement of silicon photomultipliers pulse amplitude versus light intensity will show increasing departure from proportionality as the light intensity becomes larger. A simple correction based on an initial calibration can restore the linearity provided the losses are not a large fraction of all incident photons [4].

The development of silicon photomultipliers is fast and the technology and characteristic are changing. The last few years large improvements have been achieved, mostly regarding noise, surface size and photon detection efficiency [4]. The advancement has been pushed forward by the positron emission tomography-industry (PET) where many manufactures makes their product digital by replacing photomultiplier tubes with silicon photomultipliers. This is done because of the silicon photomultipliers insensitivity of magnetic fields and this is necessary at PET/MR systems.

2.6 Construction of the detector

All scintillation detectors must be protected from ambient light and is covered by a light shielding material [4]. The material must be thin in order to minimize the attenuation of incoming gamma particles. Optical grease with a refractive index as for the detectors is used and without this there is a risk for air gap. Air has a refractive index of 1 which is far from the refractive index of the detector.

3. Materials and methods

3.1 Construction of the detector

The plastic scintillator used was NE102A with a density of 1.032 g/cm^2 and a refractive index of 1.581 [4]. The emission spectrum and additional information can be seen in Appendix A. The thickness of the plastic scintillator disc was chosen to 15 mm due to the range of the beta particle from Y-90 calculated with equation 1 resulting in a range of 12.2 mm. The scintillator was polished at the side area and unpolished at the top and bottom areas.

The optical grease used was DowCorning® 7 Release Compound [12]. A thin layer of optical grease was applied on the edge of the scintillator disc. The wavelength shifting fibre used was BCF-92 [11] from Saint Gobain with 1 mm diameter and 1.5 meter long with FC-connectors mounted at the ends of the fibre. The absorption and emission spectrum and additional information can be seen in Appendix B. The WLS fibre was wired two and a half rounds on the edge and visual inspection was done to see that the optical coupling between the fibre and the optical grease was good.

A 12 mm wide white thread sealing tape made from polytetrafluoroethylene (PTFE) was used for reflection and to hold the fibre in place. The tape covered all surfaces of the scintillator and the fibre from the scintillator to the FC-connectors for light reflection. A 19 mm wide black electrical tape meant for professional was used to cover all the white tape for sealing ambient light.

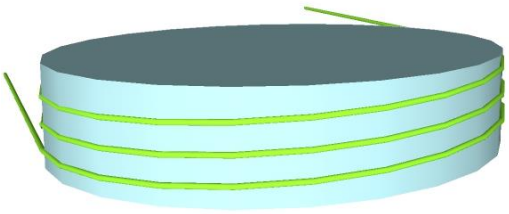

Figure 4.Wavelength shifting fibre BCF-92 wired around plastic scintillator disc NE102A.

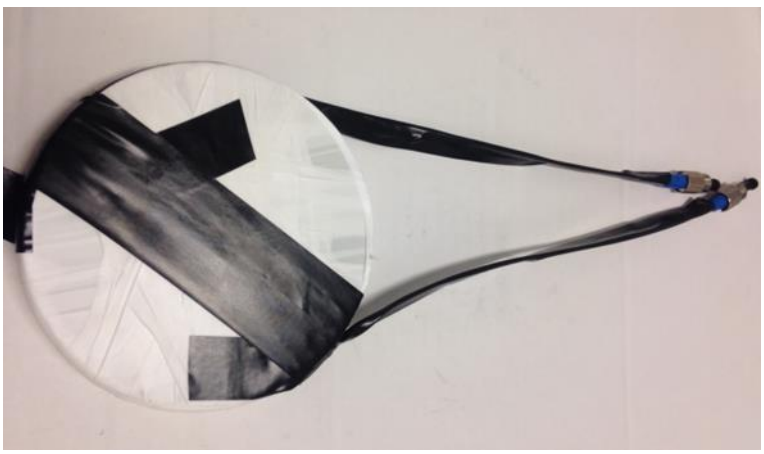

Figure 5. White thread sealing tape and black electrical tape surrounding the plastic scintillator disc NE102A.

3.2 CAEN SP5600 Educational kit

The CAEN SP5600 Educational kit consists of a power supply and amplification unit, a desktop digitizer, two sensor holders with embedded SiPM and spectrometer with three different types of detectors. The *SP5600 General Purpose Power Supply and Amplification Unit* have a wideband amplifier with 1 to 50 dB gain with step of 1 dB. The *DT5720A Desktop Digitizer* has a 250 mega-samples per second sampling rate and a digital pulse processing firmware installed. The two *SP5650A Sensor Holder with embedded SiPM* has one Hamamatsu SiPM S10362-11-100C in each sensor holder with 1x1 mm^2 active area with a temperature feedback sensor embedded. The photon detection efficiency as a function of wavelength is seen in Appendix C. The power supply and amplification unit and the desktop digitizer are sharing a 120 V power supply [12].

The mini spectrometer was Hamamatsu SiPM S10362-33-050C with a 3x3 mm^2 active area in a sensor holder made possible for coupling small detectors. The photon detection efficiency as a function of wavelength is seen in Appendix D. The detectors available were all 3x3x15 mm^3 and polished on all sides and coated with a white epoxy layer on 5 faces. The detectors were BGO (Bismuth Germanate), LYSO(Ce) (Cerium-doped Lutetium Yttrium Orthosilicate) and CsI(Tl) (Thallium-doped Cesium Iodide) [14].

The CAEN SP5600A Educational kit was connected to a laptop PC via two USB cables and the *SiPM_ControlSoftware_00_19.vi* was used. The spectrum was saved from the software to the computer in ASCII format (American Standard Code for Information Interchange) and data was analysed in Microsoft Office Excel 2010. The spectrum was modified by a logarithmic y-axis and the x-axis was cut to display relevant information.

3.3 Detector measurements

3.3.1 Setup

The measurements were performed in a room without ambient sunlight at ground level at Skåne University Hospital in Malmö, Sweden. The set-up was placed on a wooden table, 75 cm high, with the scintillator disc horizontal. The entrance window was directed to the roof. The background measurements were done without any radioactive sources present with time of measurements corresponding to the measurements with radioactive sources to be able to correct for the 0.1 µSv/h background.

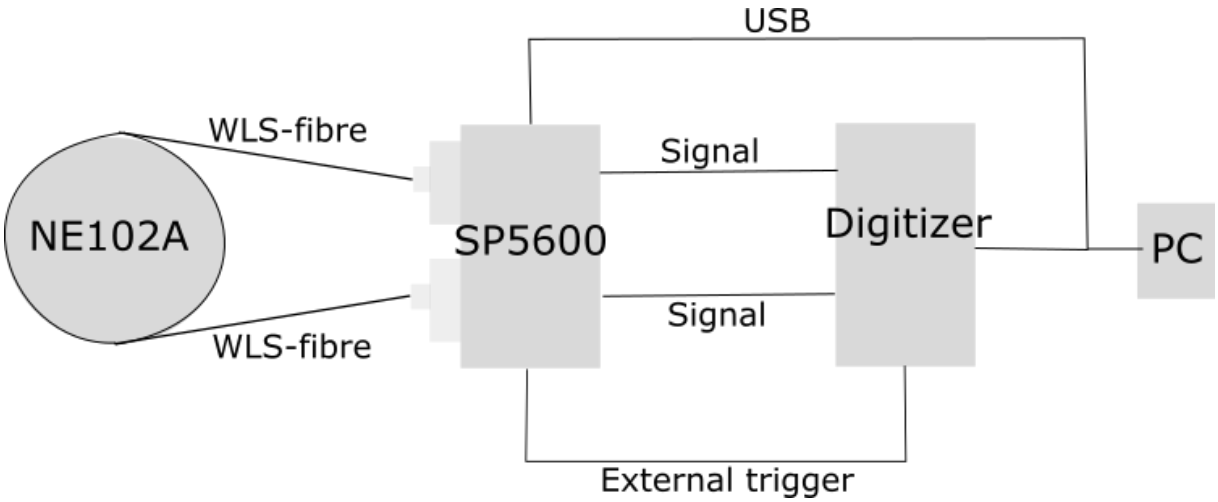

Figure 6. Block scheme of the setup including plastic scintillator NE102A, WLS-fibre BCF-92, SP5600 General Purpose Power Supply and Amplification Unit, DT5720A Desktop Digitizer, two signal cable, trigger cable and two USB-cables connected to a PC.

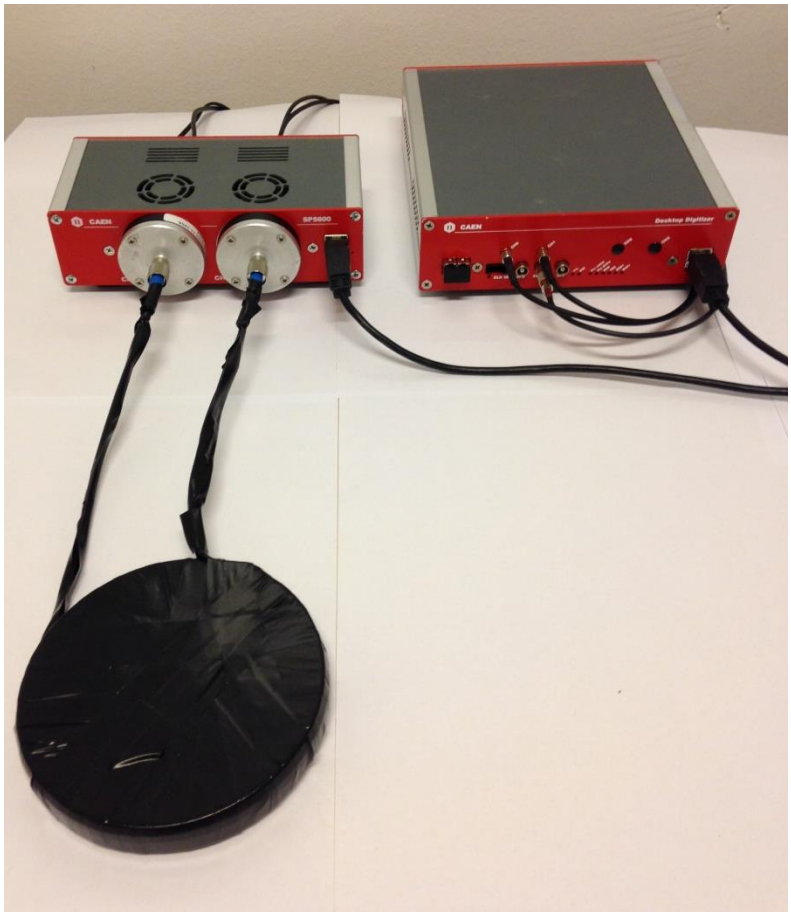

Figure 7. Light protected plastic scintillator NE102A with WLS-fibre BCF-92 connected with FC-connectors to SP5600 General Purpose Power Supply and Amplification Unit. The signal from SP5600 is processed in DT5720A Desktop Digitizer and two USB-cables are connected to a PC.

To find the optimal settings for low background rate and high count rate from Sr-90/Y-90 the parameters seen in Table 2 was varied. All the parameters were varied between suitable values seen in Table 2 and the sum of counts was noted and compared. The value of each

parameter was chosen where the count rate of background corrected Sr-90/Y-90 was the highest and the shape of the spectrum looked like a beta spectrum.

Table 2. Parameters varied in the CAEN SP5600 kit for the Hamamatsu SiPM S10362-11-100C

Component	Category	Parameter	Measured values
PSAU	Bias	Bias voltage [V]	70.47, 70.63, 70.90, 70.93, 71.20
	Gain	Gain [dB]	10, 15,20, 30, 40, 50
Digitizer		Threshold [mV]	0-90, steps of 10
	Trigger	Trigger	External, internal
		Mean [#]	1, 8, 32
		Rise time [ns]	0, 8, 80, 256
	Gate	Gate [ns]	48, 200, 504, 752, 1000, 2000, 3000, 5000
		Pre gate [ns]	0, 120, 184, 248, 384, 440, 496
		Hold-off [ns]	504, 1000, 3000, 5000, 10000
	Baseline	Mean [#]	0, 8, 32, 64, 512, 2048
		Threshold [mV]	0, 4, 8, 25, 50, 60, 75, 100
		No flat [ns]	504, 1000, 3000, 5000, 10000
	Histogram	Number of bins [#]	500, 1000, 3000
		Bin size	1, 8, 64

The two channels had different behaviour with the same setup which discarded the possibility to use two channels so channel 1 was used. The bias voltage was set to 70.63 V where the real bias voltage was pending between 70.47 V and 70.60 V. The bias voltage was set to achieve low count rate of the background and high count rate when a radioactive source is present. The count rate is monitored by the software through "PSAU counting" displaying frequency with time. Stable operating temperature was 25.4 -25.6 degrees Celsius and the parameters chosen are seen in Table 3.

Table 3. Parameters used in the CAEN SP5600 kit for the Hamamatsu SiPM S10362-11-100C.

Component	Category	Parameter	Used values
PSAU	Bias	Bias voltage [V]	70.63
	Gain	Gain [dB]	20
Digitizer		Threshold [mV]	-50
	Trigger	Trigger	Internal
		Mean [#]	16
		Rise time [ns]	8
	Gate	Gate [ns]	504
		Pre gate [ns]	0
		Hold-off [ns]	504
	Baseline	Mean [#]	16
		Threshold [mV]	8
		No flat [ns]	512
	Histogram	Number of bins [#]	1000
		Bin size	8

3.3.2 Radionuclides

All measurements with the plastic scintillator, except from the uniformity measurements described in section 3.3.3, were performed by placing the radioactive sources on top of the scintillator disc centre.

The radioactive sources that were used for measurements are listed in Table 4 where the radionuclide, activity, type of source, window of the source, measurement time and distance for the radionuclides is noted.

Table 4. Activity, type of source, window of the source, measurement time and distance for the radioactive sources that have been used for measurements.

Radionuclide	Activity at the measurement	Type of source	Window of the source	Live time [s]	Distance between source and detector [cm]
Co-60	11.7 MBq	Isotropic	Encapsulated from β	600	0.1
Cs-137	30.2 MBq	Isotropic	Encapsulated from β	600	0.1
Cs-137	133 kBq	Disc source	Thin window	600	0.1
Sr-90/Y-90	69.1 MBq	Collimated	Thin window	600	0.1
Sr-90/Y-90	3 kBq	Disc source	Thin window	600	0.1

3.3.3 Uniformity

To test the uniformity the collimated 69.1 MBq Sr-90/Y-90 source was placed at five different locations on the surface of the plastic scintillator disc seen in Figure 8. The live time was 180 seconds and number of counts was noted.

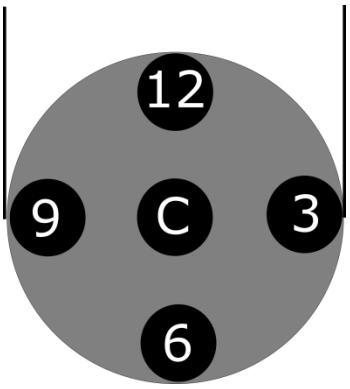

Figure 8. The numbers and letter describing the five locations where the Sr-90/Y-90 source was placed. The black lines are representing the WLS-fibre connected to the CAEN system.

3.3.4 Protection from ambient light

The plastic scintillator setup was used with the parameters seen in Table 3. For each spectrum, two measurements were done, one with ambient light present and one without. The spectrum where ambient light was present was subtracted with the spectrum without light present.

3.3.5 Temperature dependence

To test the temperature dependence, the CAEN system was started and the settings seen in Table 3 were used. Data was collected during five temperature intervals, seen in Table 5, and the number of counts per second from the background was noted.

Table 5. Temperature interval used when testing temperature dependence.

Temperature interval [ºC]
21.0-22.0
22.1-23.0
23.1-24.0
24.1-25.0
25.4-25.6

3.3.6 Direct measurements by the SiPM

The FC connectors from the plastic scintillator setup were unplugged and the opening of the sensor holder was covered with black tape to protect from ambient light. A 69.1 MBq Sr-90/Y-90 source was used and directed to the 1x1 mm^2 Hamamatsu SiPM S10362-11-100C in the sensor holder.

3.4 Spectrometer

The measurements with the mini spectrometer in the CAEN SP5600 kit was done with the three detectors; BGO, CsI(Tl) and LYSO. Optical grease was put on the 3x3 mm^2 face that wasn´t coated and was coupled to the 3x3 mm^2 Hamamatsu SiPM S10362-33-050C. The settings are seen in Table 6. The 3 kBq disc source Sr-90/Y-90 and 133 kBq disc source Cs-137 were used.

Table 6. Parameters used in the CAEN SP5600 kit for the Hamamatsu SiPM S10362-33-050C.

Component	Category	Parameter	Used values
PSAU	Bias	Bias voltage [V]	71.0
	Gain	Gain [dB]	28
Digitizer		Threshold [mV]	-60
	Trigger	Trigger	Intern
		Mean [#]	8
		Rise time [ns]	8
	Gate	Gate [ns]	280
		Pre gate [ns]	120
		Hold-off [ns]	504
	Baseline	Mean [#]	2048
		Threshold [mV]	20
		No flat [ns]	512
	Histogram	Number of bins [#]	2000
		Bin size	64

4. Results and discussion

4.1 Radionuclides

Figures 9, 10, 11 and 12 display background corrected spectra from a 69.1 MBq Sr-90/Y-90 collimated source, a 30.2 MBq Cs-137 isotropic source and an 11.7 MBq Co-60 source obtained with a live time of 600 seconds with a plastic scintillator, WLS-fibre and CAEN SP5600 kit with Hamamatsu SiPM S10362-11-100C. Figure 13 displays a background spectrum obtained with the same setup and live time.

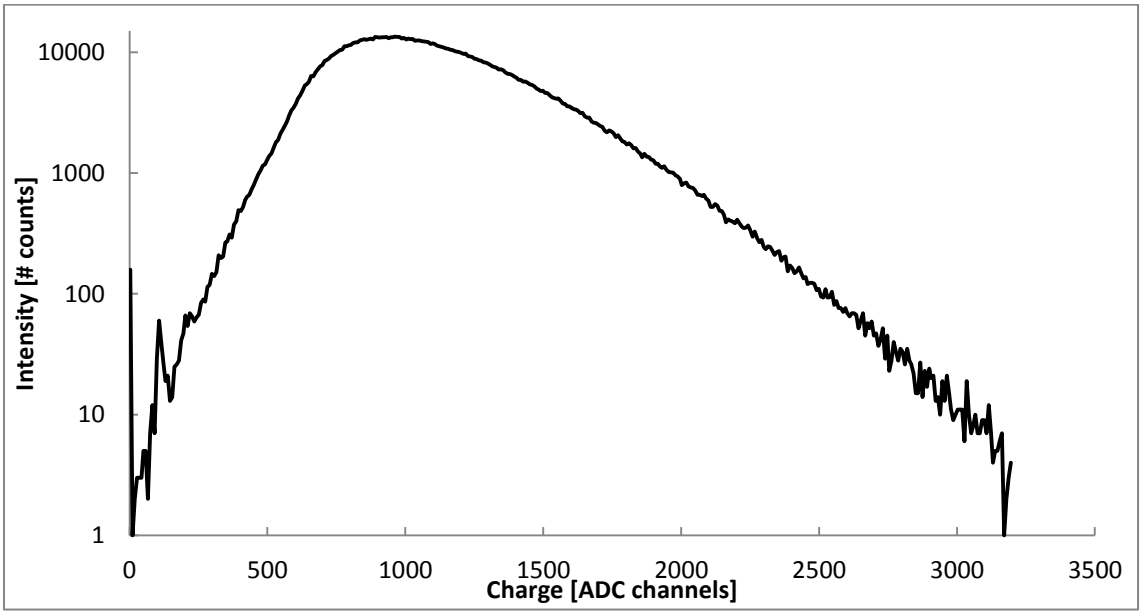

Figure 9. Background corrected spectrum of a 69.1 MBq collimated Sr-90 source with a logarithmic y-axis collected using a Hamamatsu SiPM S10362-11-100C with 600 seconds live time.

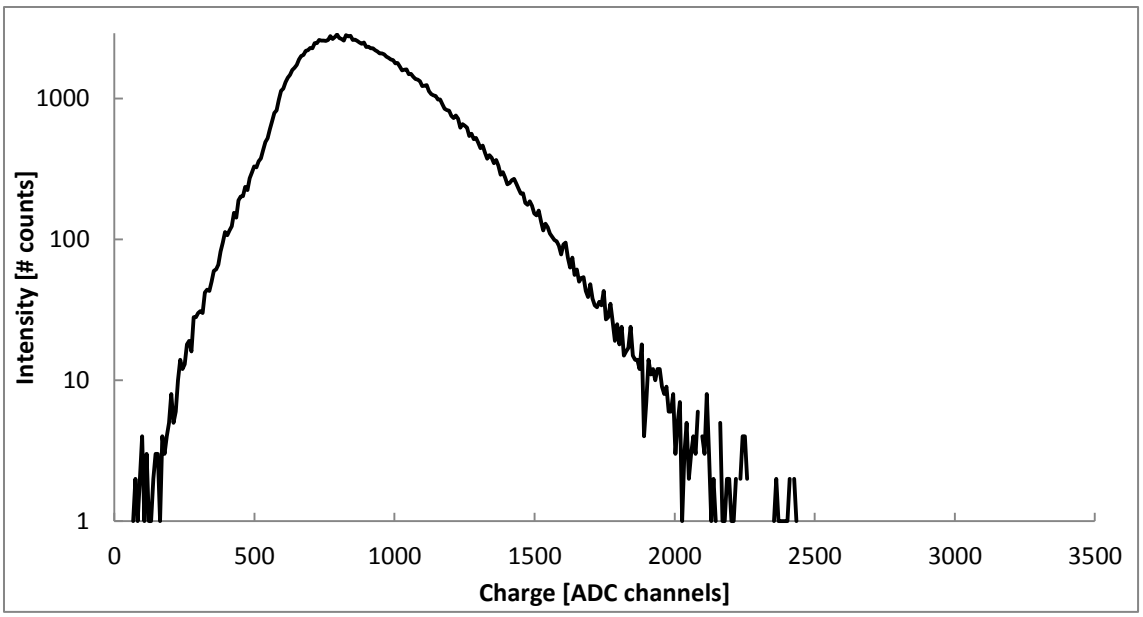

Figure 10. Background corrected spectrum of a 30.2 MBq isotropic Cs-137 source with a logarithmic y-axis collected using a Hamamatsu SiPM S10362-11-100C with 600 seconds live time.

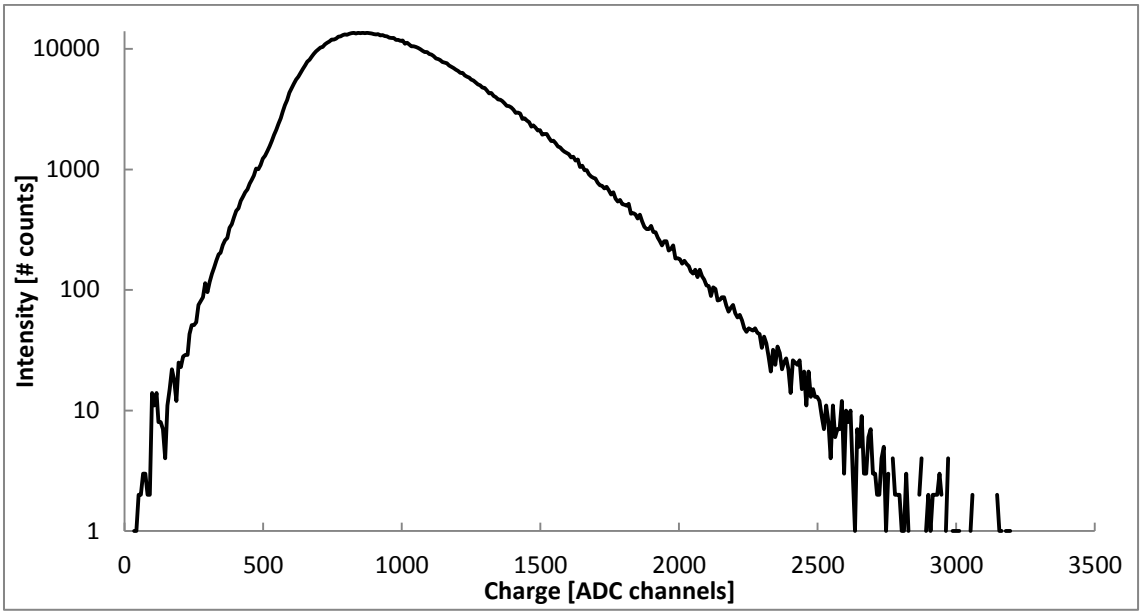

Figure 11. Background corrected spectrum of 11.7 MBq Co-60 with a logarithmic y-axis collected using a Hamamatsu SiPM S10362-11-100C with 600 seconds live time.

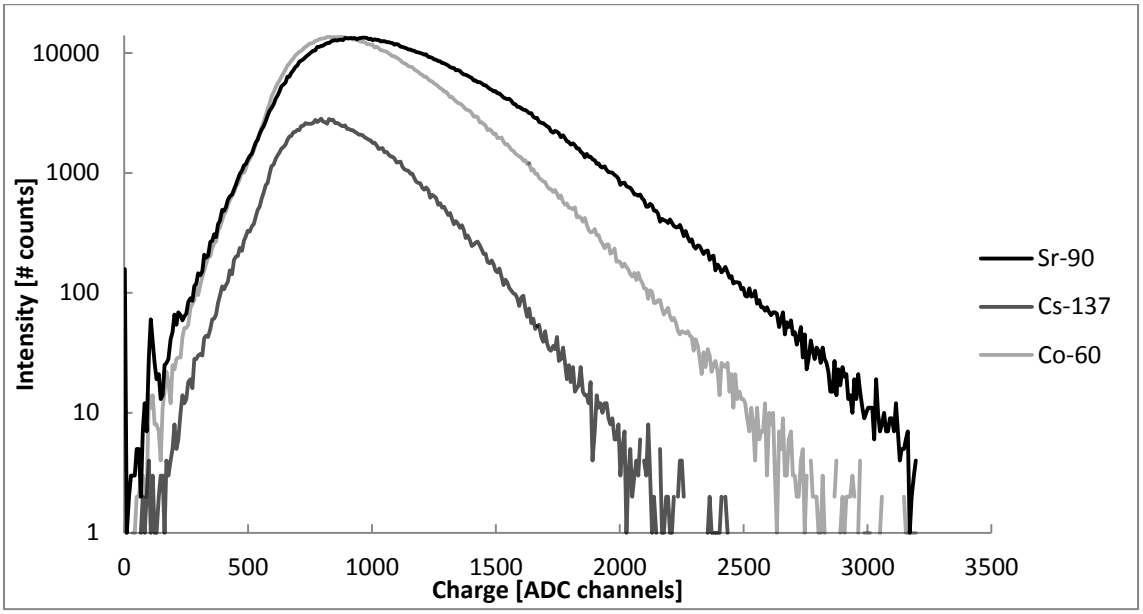

Figure 12. Comparison between background corrected spectra of 69.1 MBq Sr90, 30.2 MBq Cs-137 and 11.7 MBq Co-60 with a logarithmic y-axis collected using a Hamamatsu SiPM S10362-11-100C with 600 seconds live time.

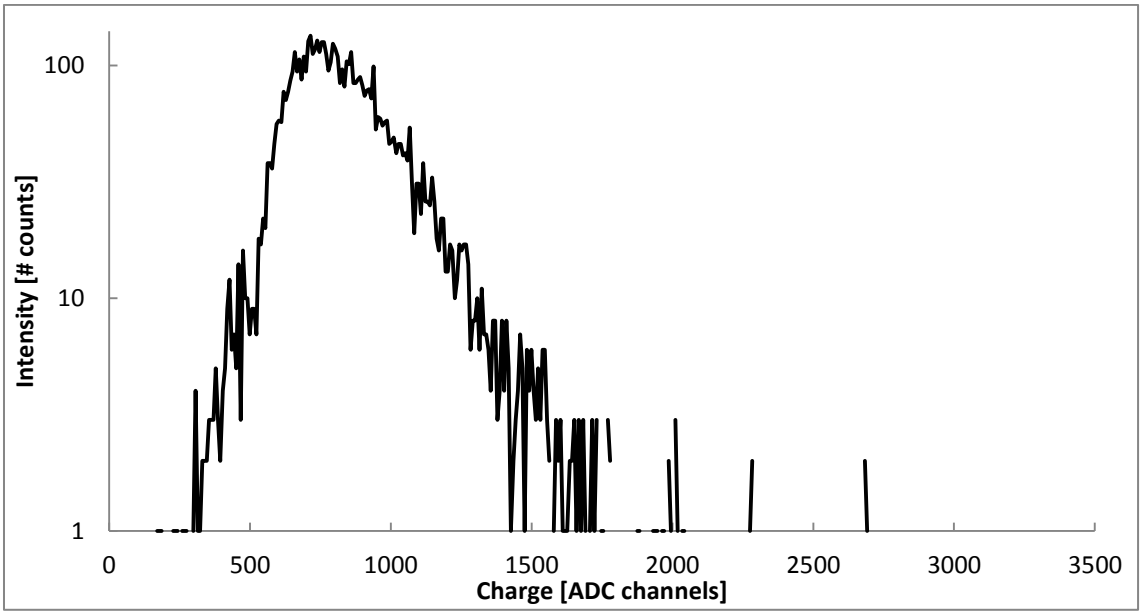

Figure 13. Background spectrum with a logarithmic y-axis collected using a Hamamatsu SiPM S10362-11-100C with 600 seconds live time.

In Figure 9 a beta spectrum from Sr-90/Y-90 is identified with a peak around channel number 950. The end-point is around channel number 3200. The beta particles from Sr-90 are identified as the beta continuum up from channel number 0 to ca 2000. The beta particles from the daughter Y-90 are also identified as a beta continuum with contribution to channel number 0 to 3200, due to the higher energy of the beta particles from Y-90. The count rate is sufficient to achieve a spectrum with good counting statistics in 10 minutes live time. Compared to the background measurement in Figure 13 the contribution from Sr-90 and Y-90 is apparent.

In Figure 10 the Compton continuum from Cs-137 is identified between channel number 0 and 2400. The full energy peak 661.7 keV could not be identified due to the thin scintillator disc of only 15 mm and the low probability for full energy absorption. The contribution from the beta particles from Cs-137 couldn't be identified due to the metal encapsulation of the Cs-137 source.

In Figure 11 a Compton continuum is identified between channel numbers 0 and 3000. The beta particles with maximum energy of 310 keV can´t escape the source due to the 3 mm steel housing. The full energy peaks of the 1173 keV and 1333 keV gamma photons are not identified due to the thin scintillator disc of only 15 mm and the low probability for full energy absorption. The contribution from the beta particles from Co-60 couldn't be identified due to the metal encapsulation of the Co-60 source.

The shape of the spectrum in Figure 12 differs between Sr-90/Y-90, Cs-137 and Co-60. The shape is similar but the difference is the energy. Sr-90/Y-90 contributes at the highest channel number due to the high energy of the beta particles from Sr-90 and Y-90 with maximum energy of 546 keV and 2280 keV respectively. Co-60 has a similar shape, but at lower channel numbers where the contribution are from the Compton continuum from the two 1173

keV and 1333 keV gamma photons. Cs-137 has a contribution from Compton from the 661.7 keV gamma photon. There is a difference in count rate where Sr-90/Y-90 has the highest count rate followed by Co-60 and Cs-137. The thickness of 15 mm of the scintillator disc makes all beta particles from Sr-90 and Y-90 to interact with the material. This combined with highest activity of the three sources explains the highest count rate of Sr-90/Y-90. The relative high contribution from Co-60 is from the Compton continuum from the two high energy gamma photons. The high energy of these particles contributes to a high energy Compton continuum and only a small part is discriminated by the threshold. Cs-137 should have the second highest count rate due to the relative high activity of 30.2 MBq but the contribution was the lowest. This could be because of the low energy part of the Compton continuum where a large part in the lower channel numbers is discriminated by the threshold. In a situation where Sr-90/Y-90, Cs-137 and Cs-60 were present in activity ratio similar to those in Figure 12, Sr-90/Y-90 can be detected due to the high contribution from Y-90 in the higher channels.

In Figure 13, a background spectrum is identified with a peak around channel number 700 with around 130 counts. A notable contribution, exceeding 5 counts, is identified up to channel number 1500 with only a few counts per channel at higher channel numbers. The noise might be from high energy muons origins from cosmic rays, ambient light photons, naturally occurring nuclides and electronic noise from the CAEN SP5600 kit. The contribution from noise is often identified among the lower channel number but this is not the case here due to the discrimination level. The discriminator level is discriminating this low level noise and the contribution from this is not identified in Figure 13. The count rate is so low that this will not interfere with measurement of radionuclides measured in Figures 9, 10, 11 and 12. The contribution of higher channel number for Sr-90/Y-90, Cs-137 and Co-60 are low, but is at higher channel numbers than the background identified in Figure 13.

4.2 Uniformity

Table 7 is displaying the count rate of background from a 69.1 MBq Sr-90/Y-90 collimated source placed in five different locations respectively on the top of the plastic scintillator disc. The mean and deviation of the mean are also displayed.

Table 7. Measurement of background and 69.1 MBq Sr-90/Y-90 in five places to test uniformity. Counts per second during 180 seconds live time with deviation from mean value.

	Background	C	12	3	6	9	Mean
Cps	8,7	2171.5	2143.5	2136.3	2148.2	2138.9	2147.7
Deviation [%]		1.1	– 0.2	– 0.5	0.02	– 0.4	0

The five different locations on the plastic scintillator disc all display a count rate within the standard deviation of the mean. The highest count rate is obtained when placing a source at the centre and is the preferred location. The other four locations yields lower count rates but are within the uncertainty according to counting statistics. The source is collimated so it is

assumed that the beta particles are entering the scintillator disc perpendicular to the scintillator surface. All particles are assumed to interact with the scintillator and are emitting scintillation light isotropically from the particle track. This is mainly the reason why the count rates are so similar on the different locations. The size of the scintillator is also too small to contribute to a great frequency of self-absorption dependent of location. The conclusion is that the setup is uniform concerning the beta particles from Sr-90/Y-90 entering the scintillator disc surface due to the very small difference in count rate.

4.3 Protection from ambient light

Figure 14 display differences between two background measurements, one with ambient light and one without. Figure 15 display differences between two measurements of a 69.1 MBq collimated Sr-90/Y-90 source, one with ambient light and one without.

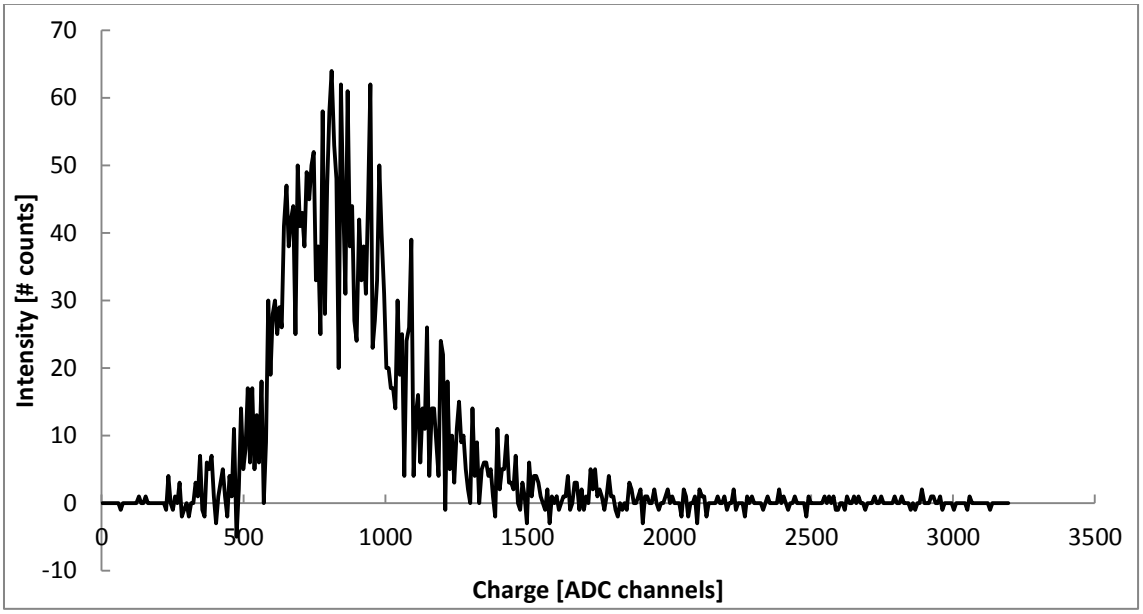

Figure 14. Background spectrum ,collected using a Hamamatsu SiPM S10362-11-100C, where measurement with ambient light are subtracted by measurement in a dark room with 600 seconds live time.

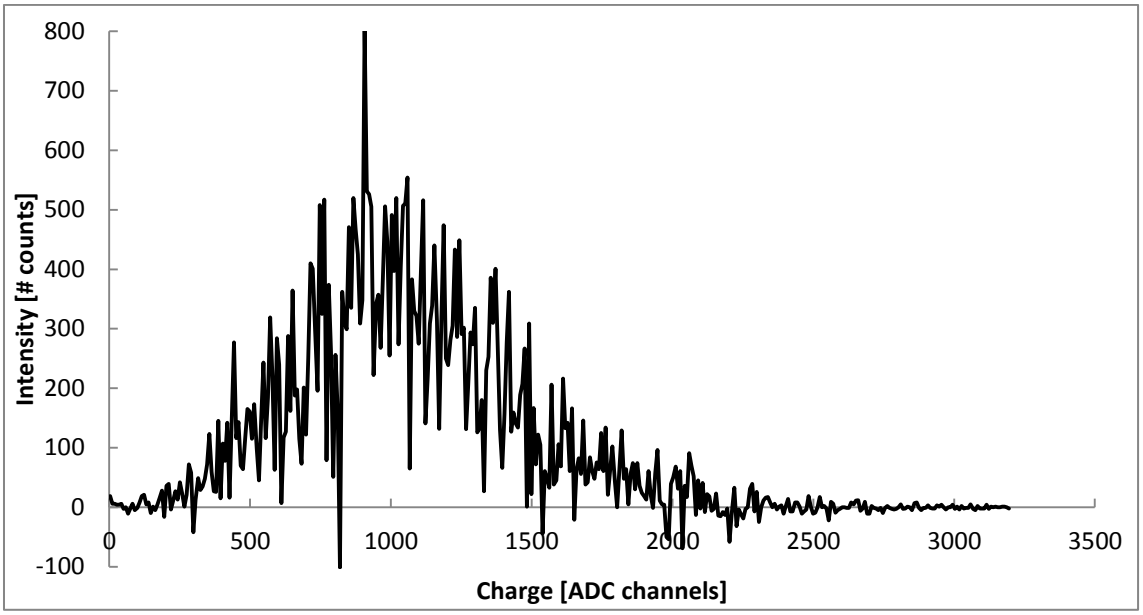

Figure 15. 69.1 MBq Sr-90/Y-90 spectrum, collected using a Hamamatsu SiPM S10362-11-100C , where a measurement with ambient light are subtracted by a measurement in a dark room resulting in the difference of ambient light present or not. The live time was 600 seconds.

In Figure 14 the background spectrum displays a notable contribution from ambient light between channel numbers 500 and 1500. Compared to the background spectrum in Figure 13 the impact of light has the same shape as for the noise identified in the measurements in dark. The conclusions are that ambient light affects the background and the setup is not completely protected from ambient light. The shape of the spectrum in Figure 13 is indicating that the contribution from ambient light is of the same shape as the noise from the background. The contribution above channel number 1500 can be explained by counting statistics due to the equal distribution around zero counts.

In Figure 15 the background corrected Sr-90/Y-90 spectrum displays a notable contribution from ambient light between channel numbers 250 to 2000. Compared to the spectrum in Figure 14 the contribution from light is greater in Figure 15, approximately tenfold. The distribution in counts is more spread in Figure 15 than in Figure 14 and can be explained by counting statistics. The setup of the experiment was identical so the added contribution must originate from the Sr-90/Y-90 source. According to counting statistics the distribution of counts should be equal around zero and not yield a positive contribution. The 69.1 MBq Sr-90/Y-90 source are contributing a very strong signal and the automatic trigger could trigger on noise in a greater extent compared to the measurement of the background. It is then important to protect the setup from ambient light when measurements of a Sr-90/Y-90 source due to the higher contribution identified in Figure 15 compared to Figure 14.

4.4 Temperature dependence

Table 8 displays counts per second for background measurements of different temperature interval when the CAEN SP5600 kit is started until stable temperature.

Table 8. Counts per seconds for background measurements for different temperature interval of the power supply amplification unit.

Temperature interval [ºC]	Counts per second
21.0-22.0	219.3
22.1-23.0	144.3
23.1-24.0	61.7
24.1-25.0	18.3
25.4-25.6	6.8

In Table 8, the count rates from the background measurements are lower with longer period of time after start-up of CAEN SP5600 kit, leading to higher temperature. The count rate is constant when the stable temperature of 24.4-25.6 is reached measuring 6.8 counts per second. It is assumed that the period of time, approximately 15 minutes, was too short to affect the response over time. The gain of the SiPM is very sensitive to operating temperature and the count rate in the temperature interval is approximately a factor thirty higher compared to the stable operating temperature of 25.4 to 25.6 degrees Celsius. To minimize the influence of the background in measurements it is important to perform the measurements when a stable operating temperature is acquired.

4.5 Direct measurements by the SiPM

Figure 8 displays measurements of 69.1 MBq collimated Sr-90/Y-90 source allowing the beta particles hit the Hamamatsu SiPM S10362-11-100C directly respective via plastic scintillator and WLS-fibre to the same SiPM.

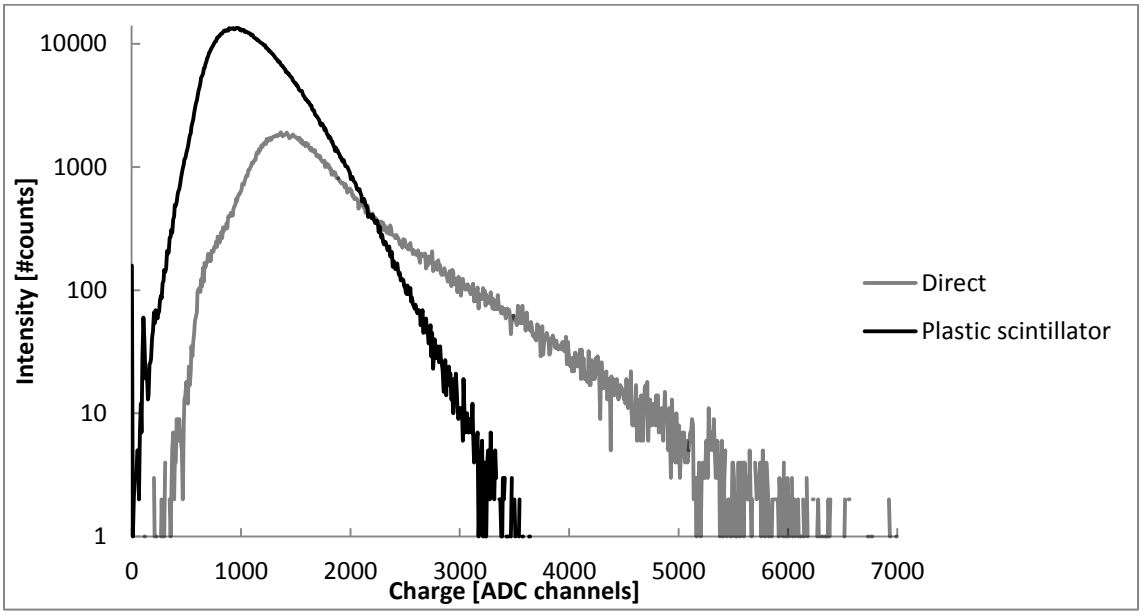

Figure 16. Background corrected 69.1 MBq Sr-90/Y-90 direct to SiPM as well as to SiPM via plastic scintillator with a logarithmic y-axis collected using a Hamamatsu SiPM S10362-11-100C with 600 seconds live time. The x-axis can´t be compared between the two different measurements.

In Figure 16 two beta continuums from Sr-90/Y-90 are identified. The SiPM should not be able to detect beta particles directly without a scintillating material because the purpose of SiPM is detection of light. The cause is not that scintillation light will be created on its way to the SiPM due to the beta particles passing of a thin layer of tape. The contribution is supposed to originate from the beta particles entering the active region of the SiPM and creates avalanches; thus inducing a signal. The difference between the direct measurement and the measurement via plastic scintillator setup is obvious with a discrepancy of shape and count rate. The x-axis can´t be compared due to different measurements but the direct measurement has a wide beta continuum while the plastic scintillator setup yields a high and narrow beta continuum. The plastic scintillator setup has a higher count rate compared to the direct exposure of Sr-90/Y-90.

4.6 Setup

The light losses of the setup originate from many sources including the scintillator, WLS-fibre and SiPM. The shape of the scintillator is important to direct the scintillation light to the WLS-fibre. Using a scintillator disc with a flat surface will trap some of the scintillation light hitting the surface perpendicular to the surface and this will not be directed to the edges where the WLS-fibre is wired. The surface treatment is important to avoid escaping light and therefore collect as much of the scintillation light. Using white thread sealing tape will reflect a great part of the scintillation light that would escape the scintillator by absorption in the black electrical tape used for ambient light protection.

Concerning the scintillation light collection by the WLS-fibre the absorption spectrum must correspond to the emission spectrum of the scintillator and cover all surfaces where scintillation light will exit the scintillator. The absorption spectrum of the WLS-fibre used in the setup didn't correspond very well to the emission spectrum of scintillator NE102A. The emission spectrum from the WLS-fibre after the wavelength shifting doesn't correspond well to the photon detection efficiency spectrum for the SiPM. The WLS-fibre was in this setup only 1.5 meter long which allowed the edge surfaces to only be covered by WLS-fibre a sixth of the total area.

The light protection of the setup could be improved by using tape of better quality but this setup is facing same issues as for a photomultiplier tube setup.

Using a photomultiplier tube setup instead the light collection are much easier and straight forward because the possibility to couple the scintillator and light guide, commonly plexiglass, directly to the entrance window of the photomultiplier tube. But the limitation is that the shape of the scintillator must correspond to the entrance window of the photomultiplier tube and could not formed so freely compared to using a WLS-fibre together with SiPM. The use of SiPM setup gives the opportunity to shape the scintillator in various forms and therefore a wider use. Several different setups of scintillators combined with WLS-fibres could be used when measuring *in situ* connected to SiPM. This yields a variety of detectors that could be used depending on the situation.

The use of a photomultiplier tube setup yields a bulky size compared to using a SiPM setup a smaller and less sensitivity to shocks and vibrations setup is given.

The uniformity is better at the SiPM setup compared to a photomultiplier tube setup. The surface of the entrance window of a photomultiplier tube isn't uniform where the effective surface is smaller than the whole surface.

Disturbances from other nuclides could be decreased utilizing the separation between the SiPM and the scintillator. This distance could be chosen by using a shorter or longer fibre making it possible to avoid great disturbances from radionuclides in the fallout to the SiPM.

The count rate from the 69.1 MBq Sr-90/Y-90 collimated source is well above the background level so the contribution from Sr-90 and Y-90 can be seen even without background subtraction. This could be very useful as it is very hard to perform a background subtraction in a fall out situation. The possibility to perform measurements at high activities makes the setup useful when the count rate are high and when using common photomultiplier setup the dead time is an issue. The detection limit is currently relatively high but in a fallout situation the quantities of Sr-90 and Y-90 are high, in order of several MBq per square meter. There is a potential for considerable improvements. A Cs-137 source in order of MBq and without a metal enclosure allowing the beta particles to escape wasn't available. It is then not possible to conclude that a relative high quantity of Cs-137 present together with Sr-90/Y-90 will disturb Sr-90/Y-90 identification. A conclusion can be made that Compton from a relative high quantity of Cs-137 will not disturb Sr-90/Y-90 identification. This is because the high energy of the beta particles from Y-90 seen at higher channel number.

4.7 Evaluation of the CAEN SP5600 kit

The CAEN SP5600 kit included a mini spectrometer containing three different detectors. Figure F1, F2 and F3 displays background corrected spectra from measurements of 3 kBq Sr-90/Y-90 disc source and 133 kBq Cs-137 disc source respectively with a 3x3x15 mm^3 BGO-, CsI(Tl)- and LYSO-detector respectively with a 3x3 mm^2 Hamamatsu SiPM S10362-33-050C.

In Figure F1 a beta continuum from Sr-90/Y-90 is identified with a contribution between channel numbers 4500 and 30000 with a peak at channel number 8500. The full energy peak and a Compton continuum from Cs-137 is identified with a contribution between channel numbers 4500 and 18000. The full energy peak is identified at channel number 12800. The Compton continuum is identified between channel number 4500 and 10000. The full energy peak from Cs-137 is resolved due to the high density of the small BGO crystal.

In Figure F2 a beta continuum from Sr-90/Y-90 is identified with a contribution between channel numbers 4500 and 50000 with a peak at channel number 9000. The full energy peak and a Compton continuum from Cs-137 is identified with a contribution between channel numbers 4500 and 40000. The full energy peak is identified at channel number 25000. The Compton continuum is identified between channel number 4500 and 40000.

In Figure F3 a beta continuum from Sr-90/Y-90 is identified with a contribution between channel numbers 2800 and 60000 with a peak at channel number 7500. The full energy peak and a Compton continuum from Cs-137 is identified with a contribution between channel numbers 2800 and 53000. The full energy peak is identified at channel number 48500. The Compton continuum is identified between channel number 2800 and 45500.

Comparing Figure F1, F2 and F3 the shape is different where LYSO displays the most distinct full energy peak and Compton distribution. The count rate from Sr-90/Y-90 is highest from the CsI(Tl)- and LYSO-detector and lowest for the BGO-detector. The density is high enough for all detectors to absorb all beta particles so this will not affect. The light yield is low at the BGO- and higher for LYSO- and CsI(Tl)-detector. Even though the CsI(Tl)-detector has a factor two higher light yield the count rate is similar. This is because the peak emission for LYSO is closer to the peak of the photon detection efficiency for the SiPM compared to CsI(Tl)-detector. The count rate from Cs-137 is highest from the LYSO-detector followed by the BGO- and CsI(Tl)-detector. This is due to the high density, relative high light yield and peak emission corresponding to the SiPM of the LYSO-detector. The CsI(Tl)-detector has the highest light yield of the three detectors but has low density and a peak emission not corresponding to the SiPM very well.

5. Future work

Future work regarding the present setup includes improvements of light protection and light collection. A simple improvement would have been to use a SiPM of the newer generation, seen in Appendix E, where lower afterpulse, cross talk and dark count rate are provided. The setup must be prepared for the possibility of *in situ* tests. An interesting detector setup to be investigated would be a combination of SiPM and photomultiplier tube. The scintillation light are collected in two different ways and it is possible to take advantage of each technique.

6. Conclusion

It is possible to measure Sr-90/Y-90 under laboratory conditions using a plastic scintillator and a SiPM. The setup is not totally light tight but the ambient light wouldn’t disturb the measurements of radionuclides. The setup is uniform regarding collecting beta particles from a Sr-90/Y-90 source but the SiPM can yield a signal if it is hit by beta particles directly. The detection limit is relative high but in a fallout situation the quantities of Sr-90 and Y-90 are high, in order of several MBq per square meter. There is however a potential for considerable improvements. Regarding the evaluation of the CAEN SP5600 kit, the associated mini spectrometer containing a different model of SiPM together with three different types of detectors, resulted in low detection limits and easy identification and quantification of Sr-90/Y-90.

References

1. M.G. Buzinny, A. V. Zelensky, I. P. Los. *Beta-spectrometric determination of ^{90}Sr in water, milk and other samples with an ultra-low-level liquid scintillation counter. Liquid Scintillation Spectrometry 1992 (439-446).*

2. A.Tarancón, H.Bagán, J.F.García and G.Rauret. *Plastic scintillators: A Powerful Tool to Reduce Mixed Waste.* WM2008 Conference, February 24-28, 2008, Phoenix, AZ. Abstract #8225.

3. Mattsson, Sören (2013). *Utveckling av scintillerande plastdetektor för mätning av β-strålande radionuklider som exempelvis 90Sr/90Y i starka fotonstrålfält.* Malmö: Application to the Swedish Radiation Safety Authority.

4. Knoll, Glenn F. (2010). *Radiation detection and measurement*. 4th ed. Michigan: John Wiley & Sons, Inc.

5. Van der Stricht, Etienne & Kirchmann, René (2001). *Radioecology: Radioactivity and Ecosystems*. Liège: International Union of Radioecology.

6. Gordon R. Gilmore (2008). Practical Gamma-Ray Spectrometry. 2nd ed. John Wiley & Sons, Ltd.

7. Livechart – IAEA Nuclear Data Services. Available (2015-05-22): https://www-nds.iaea.org/relnsd/vcharthtml/VChartHTML.html.

8. N. Casacuberta, P. Masqué, J. Garcia-Orellana, R. Garcia-Tenorio, K. O. Buesseler. *^{90}Sr and ^{89}Sr in seawater off Japan as a consequence of the Fukushima Dai-ichi nuclear accident*. *Biogeosciences Discussions*, 2013; 10 (2).

9. F.H.Attix. (1986). *Introduction to Radiological Physics and Radiation Dosimetry*. Mörlenbach: John Wiley & Sons, Inc.

10. NOVA Technical Design Report (2007). Available (2015-05-22): http://lss.fnal.gov/archive/design/fermilab-design-2007-01.pdf

11. Scintillating Optical Fibers. Saint Gobain Crystals. Available (2015-05-22): http://www.crystals.saint-gobain.com/uploadedFiles/SG-Crystals/Documents/SGC%20Fibers%20Brochure.pdf

12. Dow Corning. (2013). *Product Information: Dow Corning® 7 Release Compound.* Available (2015-05-22): http://www.dowcorning.com/DataFiles/090276fe801901a4.pdf.

13. CAEN SP5600 kit. Available (2015-05-22): http://www.caen.it/jsp/Template2/CaenProd.jsp?showLicence=false&parent=61&idmod=719&downloadDocumentId=8213

14. Mini spectrometer. Available (2015-05-22): http://www.caen.it/servlet/checkDocumentsFile?Id=7498.

15. Saint Gobain Premium Crystals. Available (2015-05-22): http://www.crystals.saint-gobain.com/uploadedFiles/SG-Crystals/Documents/SGC%20BC400-404-408-412-416%20Data%20Sheet.pdf.

16. Datasheet Hamamatsu S10362-11-series. Available (2015-05-22): http://www.phys.hawaii.edu/~idlab/taskAndSchedule/iTOP/SciFi_doco/s10362-11series_kapd1022e05.pdf

17. Datasheet Hamamatsu S10362-33-050C. Available (2015-05-22): http://www.datasheetlib.com/datasheet/1424500/s10362-33-050c_hamamatsu-photonics.html

18. Massimo Caccia. Presentation: *Multipixel Photon Counters: introducing the digital age in low light detection*. Hamamatsu Technology Days. November 19 2014, Lund.

Appendix A

Figure A1 displays the emission spectrum of BC400 Saint Gobain, called NE102A by Nuclear Enterprises. Table A1 displays properties of BC400/NE102A.

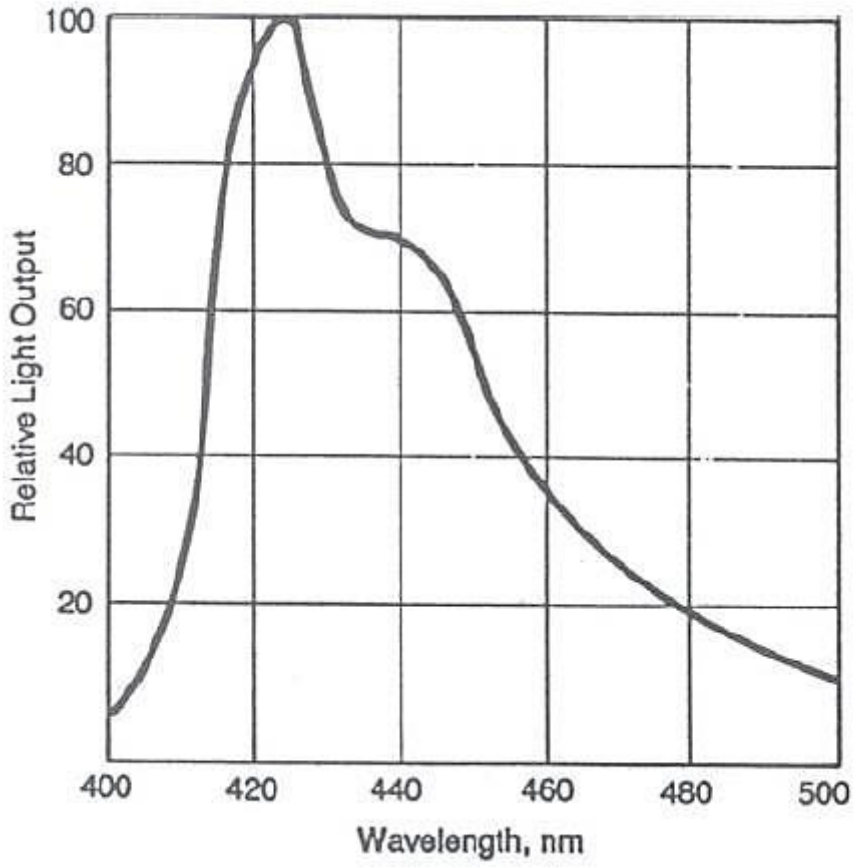

Figure A1. Emission spectrum of BC400 Saint Gobain, called NE102A by Nuclear Enterprises [15].

Table A1. Properties of the NE102A/BS-400 [4].

Nuclear Enterprises product name	St. Gobain product name	Density	Refractive index	Light output % Anthracene	Wavelength of max emission [nm]	Rise time of the signal [ns]	Decay time of the signal [ns]
NE102A	BC-400	1.032	1.581	65	423	0.6	2.4

Appendix B

Figure B1 displays the absorption and emission spectrum of the wavelength shifting fibre BCF-92. Table B1 displays the properties of the wavelength shifting fibre BCF-92.

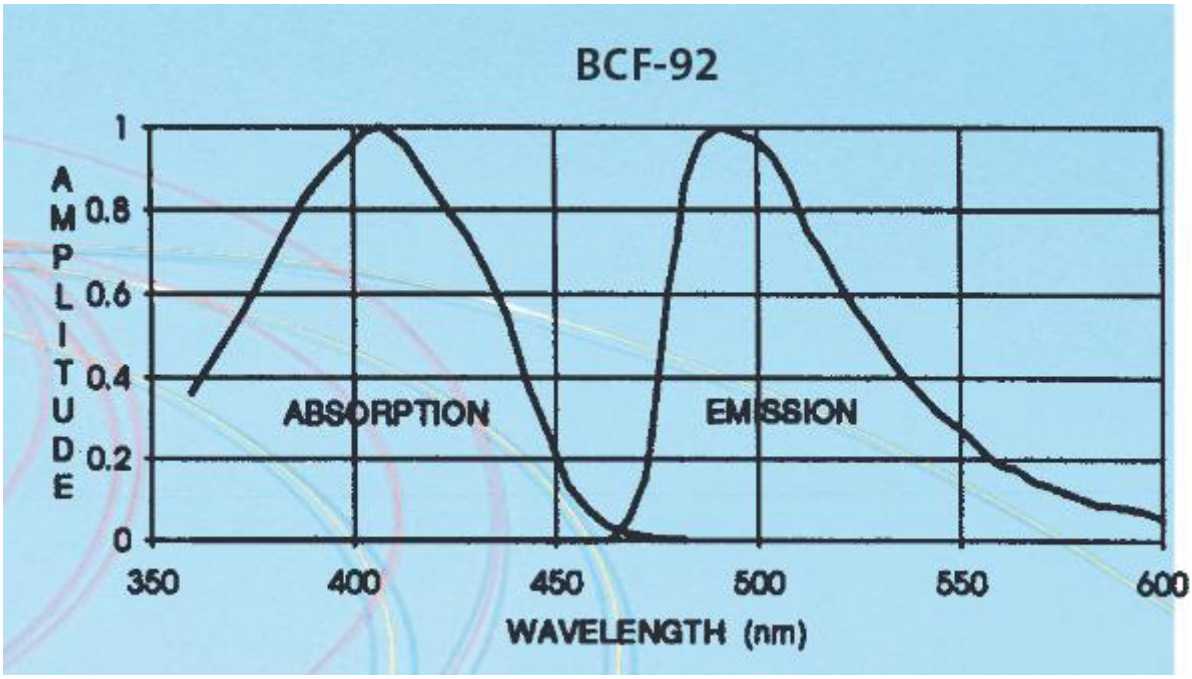

Figure B1. Absorption and emission spectrum of the wavelength shifting fibre BCF-92 [11].

Table B1. Properties of the wavelength shifting fibre BCF-92 [11].

Fibre	Emission colour	Emission peak [nm]	Decay time[ns]
BCF-92	Green	492	2.7

Appendix C

Figure C1 display the photon detection efficiency as a function of wavelength for the Hamamatsu SiPM S10362-11-100U, S10362-11-050U and S10362-11-025U. This could be compared to the S10362-11-100C, S10362-11-050C and S10362-11-025C.

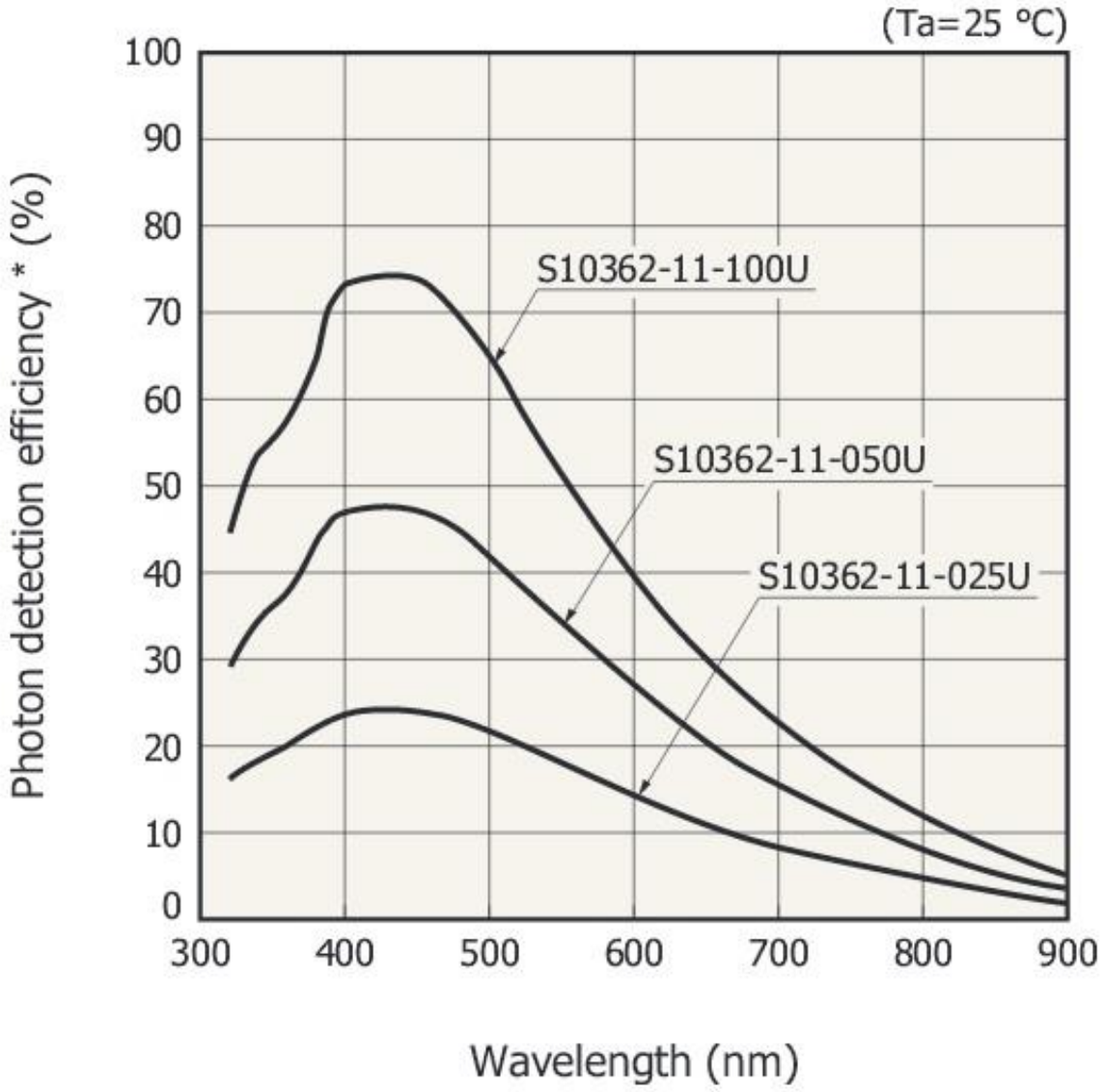

*Figure C1. Photon detection efficiency vs wavelength for Hamamatsu SiPM S10362-11-100U, -050U and 025U.*Photon detection efficiency includes effects of crosstalk and afterpulses. The photon detection efficiency is the same for the Hamamatsu SiPM S10362-11-100C , S10362-11-050C and S10362-11-025C [16].*

Appendix D

Figure D1 display the photon detection efficiency as a function of wavelength for the Hamamatsu SiPM S10362-33-050C.

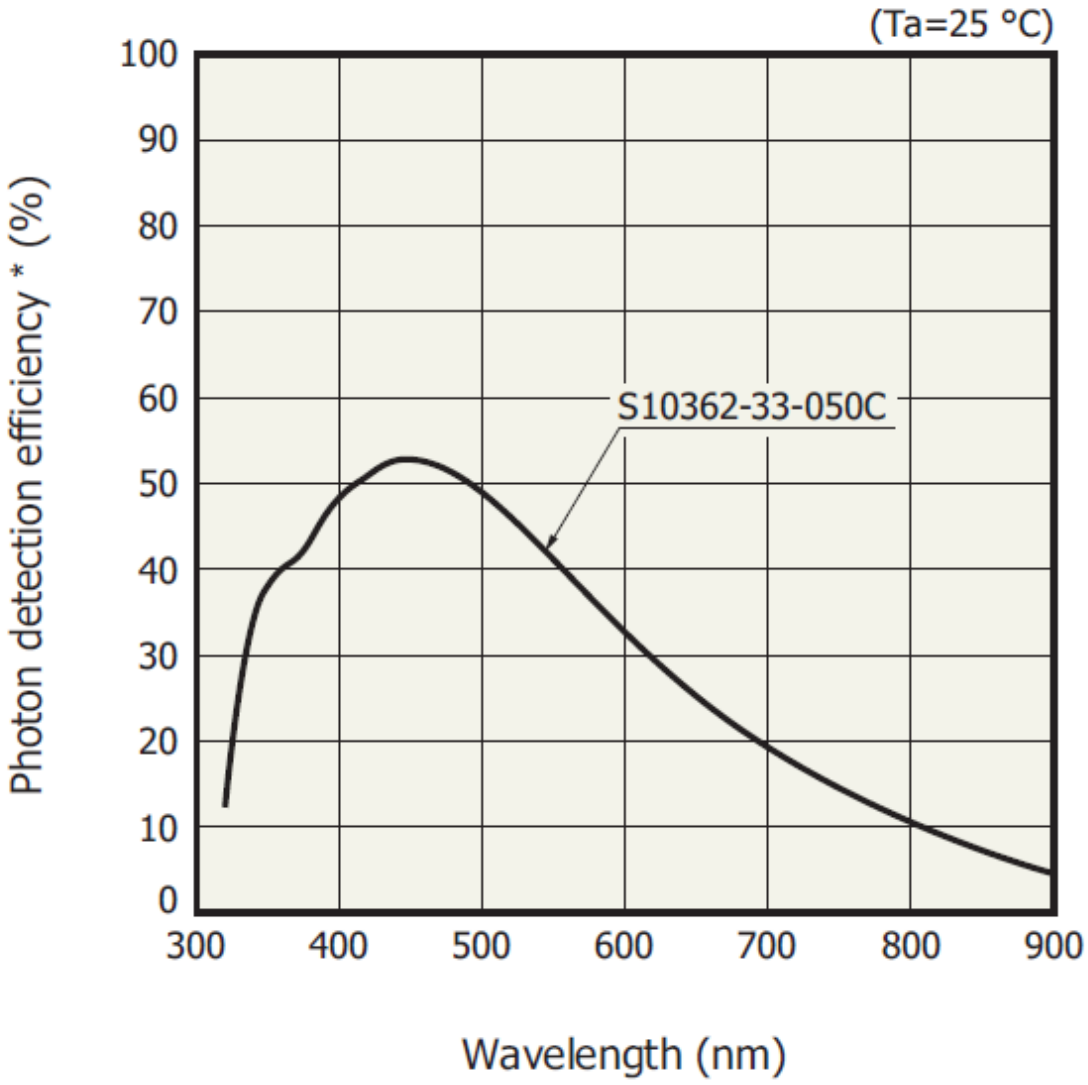

*Figure D1. Photon detection efficiency vs wavelength for Hamamatsu SiPM S10362-33-050C.*Photon detection efficiency includes effects of crosstalk and afterpulses. [17]*

Appendix E

Figure E1 and E2 displays the improvements of newer generations of Hamamatsu SiPM.

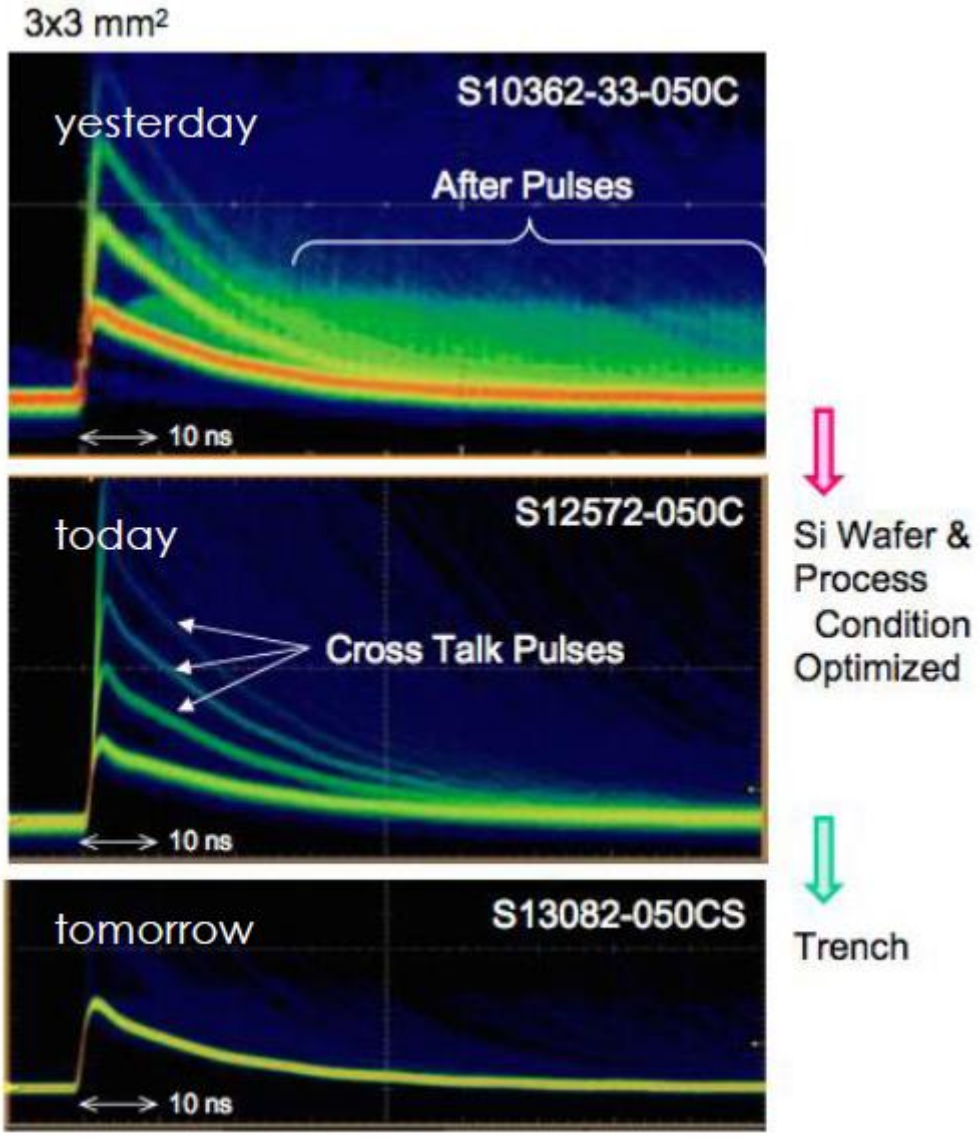

Figure E1[2]. Comparison of pulses of three SiPM from three generations where the newest generation is at the bottom with older generations above. The SiPM are irradiated with the same light source. The improvement related to after pulses and cross talk pulses are clearly demonstrated [18].

[2] Courtesy of Massimo Caccia.

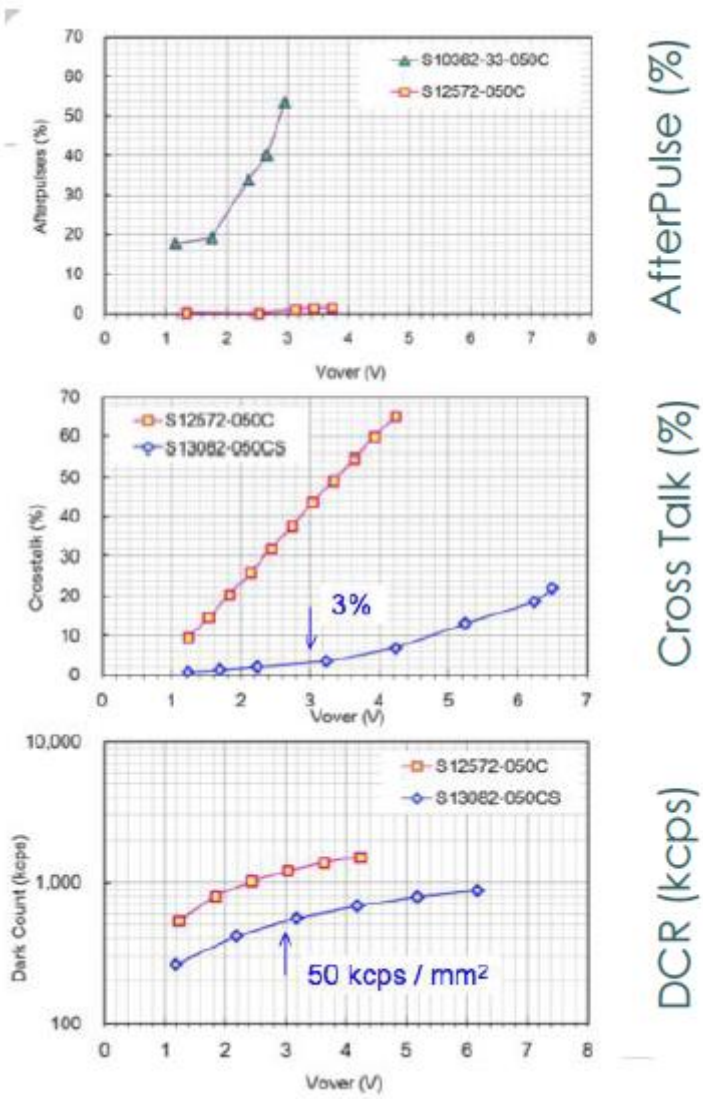

Figure E2[3]. Comparison of the newer generation Hamamatsu SiPM S10362-33-050C and S13082-050CS and older generation Hamamatsu SiPM S12572-050C respectively regarding afterpulsing, cross talk and dark count rate for overvoltage. The improvement related to after pulses, cross talk and dark count rate are clearly demonstrated [18].

[2] Courtesy of Massimo Caccia.

Appendix F

Figure F1, F2 and F3 displays background corrected spectra from measurements of 3 kBq Sr-90/Y-90 disc source and 133 kBq Cs-137 disc source. This was performed with a 3x3x15 mm^3 BGO-, CsI(Tl)- and LYSO-detector respectively together with a 3x3 mm^2 Hamamatsu SiPM S10362-33-050C.

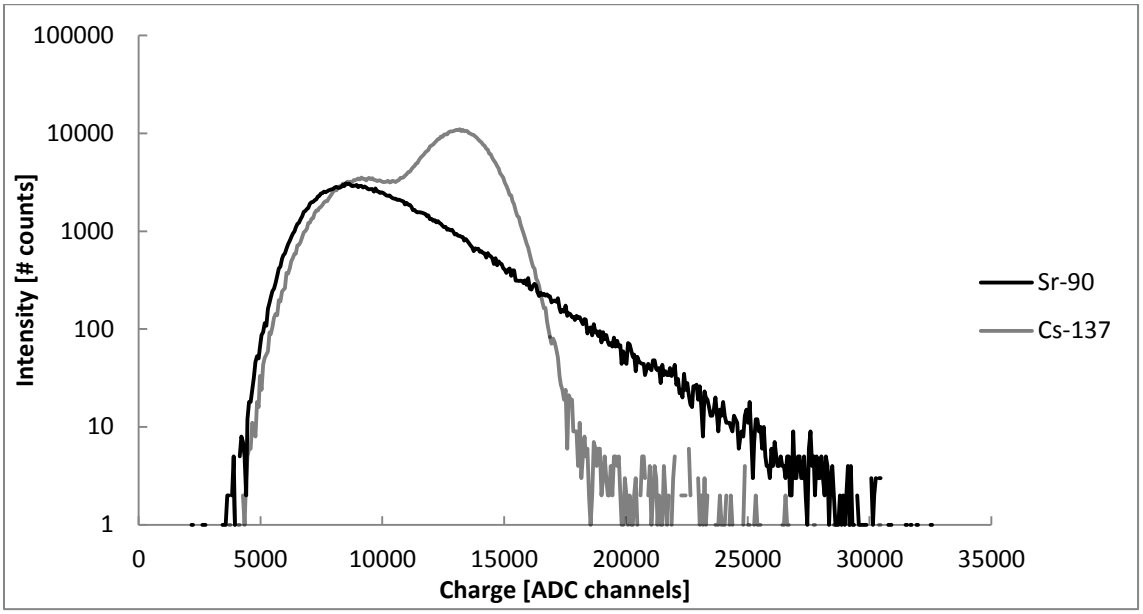

Figure F1. Background corrected spectra of two disc sources containing 3 kBq Sr-90/Y-90 and 133 kBq Cs-137. This was done with a BGO-detector and 3x3 mm^2 Hamamatsu SiPM S10362-33-050C with 600 seconds live time.

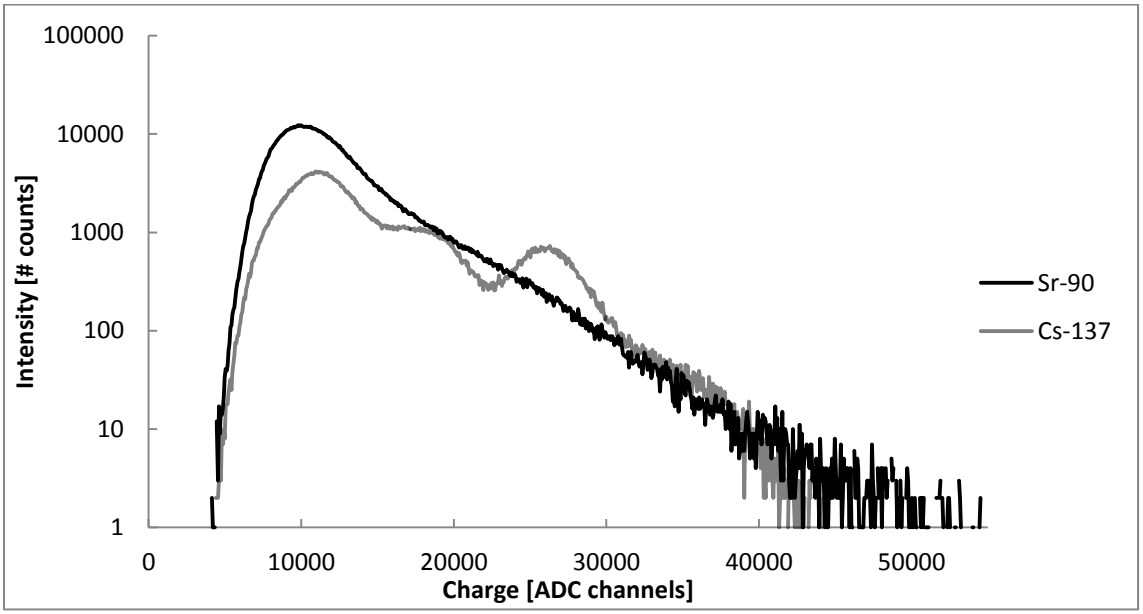

Figure F2. Background corrected spectra of two disc sources containing 3 kBq Sr-90/Y-90 and 133 kBq Cs-137. This was done with a CsI(Tl)-detector and 3x3 mm^2 Hamamatsu SiPM S10362-33-050C with 600 seconds live time.

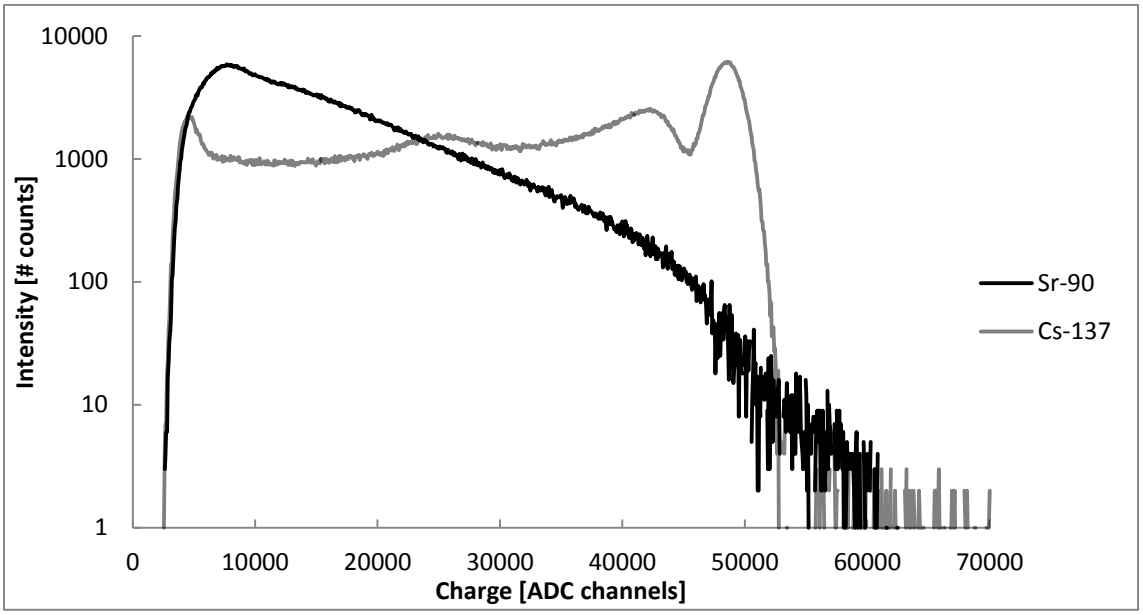

Figure F3. Background corrected spectra of two disc sources containing 3 kBq Sr-90/Y-90 and 133 kBq Cs-137. The spectra was obtained using a LYSO-detector and 3x3 mm^2 Hamamatsu SiPM S10362-33-050C with 600 seconds live time.